Bioactive Materials 6 (2021) 2711–2728

Contents lists available at ScienceDirect

Bioactive Materials

journal homepage: www.sciencedirect.com/journal/bioactive-materials

Enhancement of acellular cartilage matrix scaffold by Wharton's jelly mesenchymal stem cell-derived exosomes to promote osteochondral regeneration

Shuangpeng Jiang [a,b], Guangzhao Tian [b,c], Zhen Yang [b,c], Xiang Gao [a], Fuxin Wang [b], Juntan Li [a], Zhuang Tian [b], Bo Huang [b], Fu Wei [b], Xinyu Sang [b], Liuqi Shao [b], Jian Zhou [b], Zhenyong Wang [b], Shuyun Liu [b], Xiang Sui [b], Quanyi Guo [b,***], Weimin Guo [b,**], Xu Li [a,*]

[a] Department of Orthopedics, The First Hospital of China Medical University, 155 Nanjing North Street, Heping District, Shenyang, 110001, Liaoning Province, China
[b] Institute of Orthopedics, The First Medical Center, Chinese PLA General Hospital, Beijing Key Lab of Regenerative Medicine in Orthopedics, Key Laboratory of Musculoskeletal Trauma and War Injuries PLA, No. 28 Fuxing Road, Haidian District, Beijing, 100853, China
[c] School of Medicine, Nankai University, Tianjin, 300071, China

ARTICLE INFO

Keywords:
Articular cartilage
Regeneration
Tissue engineering
Mesenchymal stem cells
Exosomes

ABSTRACT

Articular cartilage defect repair is a problem that has long plagued clinicians. Although mesenchymal stem cells (MSCs) have the potential to regenerate articular cartilage, they also have many limitations. Recent studies have found that MSC-derived exosomes (MSC-Exos) play an important role in tissue regeneration. The purpose of this study was to verify whether MSC-Exos can enhance the reparative effect of the acellular cartilage extracellular matrix (ACECM) scaffold and to explore the underlying mechanism. The results of in vitro experiments show that human umbilical cord Wharton's jelly MSC-Exos (hWJMSC-Exos) can promote the migration and proliferation of bone marrow-derived MSCs (BMSCs) and the proliferation of chondrocytes. We also found that hWJMSC-Exos can promote the polarization of macrophages toward the M2 phenotype. The results of a rabbit knee osteochondral defect repair model confirmed that hWJMSC-Exos can enhance the effect of the ACECM scaffold and promote osteochondral regeneration. We demonstrated that hWJMSC-Exos can regulate the microenvironment of the articular cavity using a rat knee joint osteochondral defect model. This effect was mainly manifested in promoting the polarization of macrophages toward the M2 phenotype and inhibiting the inflammatory response, which may be a promoting factor for osteochondral regeneration. In addition, microRNA (miRNA) sequencing confirmed that hWJMSC-Exos contain many miRNAs that can promote the regeneration of hyaline cartilage. We further clarified the role of hWJMSC-Exos in osteochondral regeneration through target gene prediction and pathway enrichment analysis. In summary, this study confirms that hWJMSC-Exos can enhance the effect of the ACECM scaffold and promote osteochondral regeneration.

1. Introduction

The self-healing ability of articular cartilage after injury is very limited [1]. If an articular cartilage injury is not treated promptly, it can easily cause osteoarthritis (OA), which seriously endangers human physical and mental health [2]. It is estimated that 250 million people worldwide suffer from OA [3]. Unfortunately, most of the commonly used surgical techniques can regenerate only fibrocartilage, the mechanical properties of which are much poorer than those of hyaline cartilage [4]. In recent years, a tissue engineering strategy based on mesenchymal stem cells (MSCs) has been considered a promising method for articular cartilage regeneration [5]. Human Wharton's jelly-derived MSCs (hWJMSCs) are considered seed cells of tissue-engineered articular cartilage with broad prospects for

Peer review under responsibility of KeAi Communications Co., Ltd.
* Corresponding author.
** Corresponding author.
*** Corresponding author.
E-mail addresses: doctorguo_301@163.com (Q. Guo), guowm5@mail.sysu.edu.cn (W. Guo), likyoku@cmu.edu.cn (X. Li).

https://doi.org/10.1016/j.bioactmat.2021.01.031
Received 11 November 2020; Received in revised form 14 January 2021; Accepted 25 January 2021

application [6] and the advantages of strong proliferation and differentiation, a uniform immunophenotype, noninvasive acquisition procedures and no ethical controversy [7,8]. However, the storage and transportation conditions of the cells are stringent. In addition, the tumorigenicity, risk of disease transmission and possible immune rejection of MSCs hinder the application of tissue-engineered cartilage based on MSCs [9,10].

Exosomes (Exos) are extracellular vesicles 30–150 nm in diameter produced by cells through the paracrine pathway. First, it was thought that Exos were waste products produced by cells. As researchers have gradually deepened their understanding of Exos, they have become regarded as important carriers for transmitting biological signals between cells. The lipid outer membrane of Exos can protect the various encapsulated nucleic acids, proteins, lipids and other signaling molecules, enabling them to facilitate intercellular communication. Among these cargos, exosomal microRNAs (miRNAs) are believed to play an important role in the biological processes of tumor immunity [11], the inflammatory response and oxidative damage [12], apoptosis [13], and cancer metastasis [14]. Recent evidence has shown that Exos derived from MSCs (MSC-Exos) have similar biological functions to MSCs and play an important role in MSC-mediated tissue repair and regeneration [15–17]. Exos are not tumorigenic or immunogenic, circumventing the risks of MSC transplantation, and their storage and transportation requirements are less stringent than those of MSCs [18,19]. Studies have confirmed the beneficial effects of MSC-Exos in the regeneration of articular cartilage [20,21]. Therefore, MSC-Exos are considered to be ideal substitutes for MSCs in "cell-free" tissue engineering strategies [22]. The acellular cartilage extracellular matrix (ACECM) scaffold previously prepared by our research group has a vertically arranged biomimetic structure that can provide a microenvironment for stem cell adhesion, proliferation and differentiation [23–25].

To explore whether osteochondral regeneration can be achieved via "cell-free" tissue engineering, in our study, for the first time, hWJMSC-Exos were combined with the ACECM scaffold, with a suitable structure and composition, to repair osteochondral defects. Then, from the perspective of the joint cavity microenvironment, the mechanism by which Exos promote osteochondral regeneration was preliminarily explained. Finally, through miRNA sequencing and pathway enrichment, the effective components and signaling pathways through which hWJMSC-Exos may play a role in the process of osteochondral regeneration were further determined (Fig. 1).

2. Materials and methods

2.1. hWJMSC culture and identification

2.1.1. Isolation and culture of hWJMSCs

After obtaining approval from the Ethics Committee of the Chinese PLA General Hospital and patient consent, fresh human umbilical cords were obtained from pregnant women who underwent full-term cesarean section. Wharton's jelly was peeled from the umbilical cord and cut into pieces 1 mm^3 in size under aseptic conditions. Sterile gauze was placed in a cell culture flask, and pieces of Wharton's jelly were spread on the gauze. Culture medium containing 15% fetal bovine serum was added to the culture flask. The flask was placed in a constant-temperature incubator for culture. The culture medium was changed every 3 days. The cells were passaged upon reaching 90% confluence. To ensure cell viability, this experiment only used cells from passage 3 to passage 5.

2.1.2. Flow cytometry

A suspension of 1×10^6 hWJMSCs (100 μL) was placed in a centrifuge tube, and the following antibodies were used for fluorescence labeling: CD34-PE (BioLegend, 343607), CD45-PE (BioLegend, 368511), CD73-PE (Abcam, Ab155378), CD90-PE (BioLegend, 328113), and CD105-PE (BioLegend, 323207). After incubation for 30 min in the dark, the cells were washed twice with phosphate-buffered saline (PBS), and flow cytometry (BD Bioscience, BD FACSCalibur) was performed to detect the abovementioned marker proteins.

2.1.3. hWJMSC differentiation ability

According to the manufacturer's instructions, adipogenic induction medium (Cyagen Biosciences, HUXUC-90031), osteogenic induction medium (Cyagen Biosciences, HUXUC-90021) and chondrogenic induction medium (Cyagen Biosciences, HUXUC-90041) were used to culture hWJMSCs. After 21 days, oil red O staining, alizarin red staining and alcian blue staining were performed to evaluate the ability of

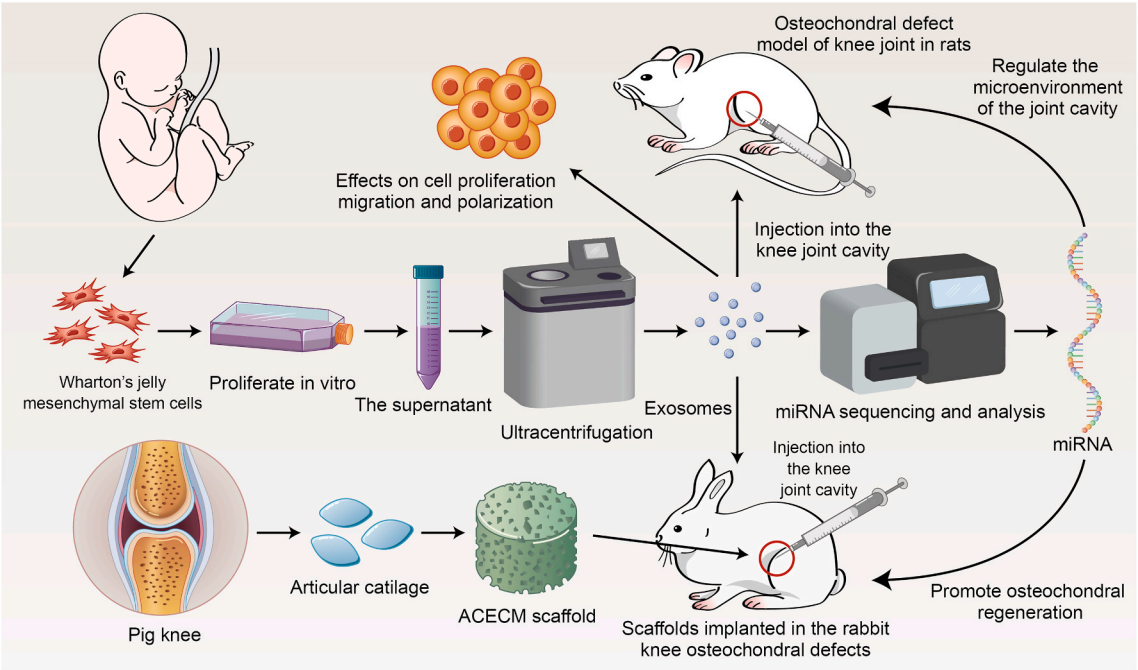

Fig. 1. Schematic illustration of the whole study.

hWJMSCs to differentiate into adipocytes, osteocytes and chondrocytes, respectively.

2.2. Extraction and identification of Exos

2.2.1. Extraction of Exos

When hWJMSCs reached 60% confluence, the culture medium was replaced with culture medium containing 10% Exo-free serum (SBI, EXO-FBS-50A-1) for 48 h, and the culture supernatant was collected. Differential ultracentrifugation was used to extract Exos (Fig. 2a). In short, centrifugal force of 300×*g*, 2000×*g*, 10000×*g*, and 100000×*g* was used to centrifuge the cell culture supernatant. The final pellet was resuspended in 200 μL of PBS. Exos were quantified using a bicinchoninic acid (BCA) protein quantification kit (Thermo Scientific, 23225).

2.2.2. Transmission electron microscopy (TEM)

Exos were loaded onto a Formvar carbon-coated EM copper mesh and stained using an Exo staining kit (101 Bio, P130) according to the manufacturer's instructions. After air-drying, a transmission electron microscope (JEOL, JEM 2100-PLUS) was used to observe the shape of the Exos.

2.2.3. Nanoparticle tracking analysis (NTA)

The Exo suspension was diluted to 1.0 mL, mixed by shaking, and then transferred to a 1.0-mL syringe. The concentration and particle size distribution of the Exos were measured using an NTA detector (Malvern Panalytical, NanoSight NS300).

2.2.4. Western blot (WB) detection

A BCA protein quantification kit was used to determine the protein concentration of Exos according to the manufacturer's instructions. According to the quantitative results, the quantity of Exos in each sample was calculated; an appropriate amount of sodium dodecyl sulfate (SDS) buffer was added, the sample was vortexed and mixed, and protein electrophoresis was performed after denaturation in 95 °C water for 5 min. After electrophoresis was completed, the separation gel was removed, and the target protein in the gel (the positive exosomal protein markers CD9, TSG101 and CD63 and the negative protein marker calnexin) was transferred to a polyvinylidene difluoride (PVDF) membrane. After blocking with a 3% bovine serum albumin (BSA) blocking solution, the membranes were incubated with the primary and secondary antibodies, developed, fixed and exposed.

2.3. Preparation and characterization of ACECM scaffold

2.3.1. Preparation of ACECM scaffold

Our group previously fabricated an ACECM scaffold with a vertically oriented structure that is biomimetic in terms of both components and structure and has been clinically applied. In brief, porcine articular cartilage was minced and decellularized using physical methods to obtain the ACECM suspension. The ACECM suspension was placed in a cylindrical mold for deep-low temperature freeze-drying and then crosslinked with water-soluble carbodiimide to prepare a porous scaffold with a vertically oriented structure.

2.3.2. Scanning electron microscopic (SEM) observation of ACECM scaffold

The cylindrical ACECM scaffold was cut into thin slices with a thickness of approximately 1 mm, exposing the transverse and longitudinal sections. The sections were adhered to a tray and covered with conductive metal powder, and after drying, their structure was observed using a scanning electron microscope (Hitachi, S-4800).

2.3.3. Cytocompatibility of ACECM scaffold

Bone marrow-derived MSCs (BMSCs) were collected from the iliac bone of 3-month-old rabbits. The methods used for the isolation and culture of BMSCs have been reported in previous articles by our group [23]. The ACECM scaffold was cut into discs with a diameter of 3.5 mm and a thickness of 1 mm. BMSCs were plated on the scaffold samples (5×10^5 cells/scaffold) and cultured in vitro. After 1, 4, and 7 days, the cell-scaffold complexes were stained with a live/dead cell staining kit, and cell viability was determined using a confocal laser microscope (Leica, TCS SP8). Finally, the cell-scaffold complexes were fixed with glutaraldehyde, and SEM observation was performed as described above.

2.4. Effect of Exos on BMSCs, chondrocytes, and macrophages in vitro

The methods for the isolation and culture of chondrocytes has been reported in previous research by our group [26]. We used 3rd generation rat chondrocytes and RAW 264.7 mouse macrophages for the experiments.

2.4.1. Effect of Exos on BMSC and chondrocyte proliferation

The cell concentration was adjusted to 5×10^4/mL; then, 100 μL per well was inoculated into 96-well plates, and the cells were cultured overnight to allow adhesion. Next, the medium was changed to serum-

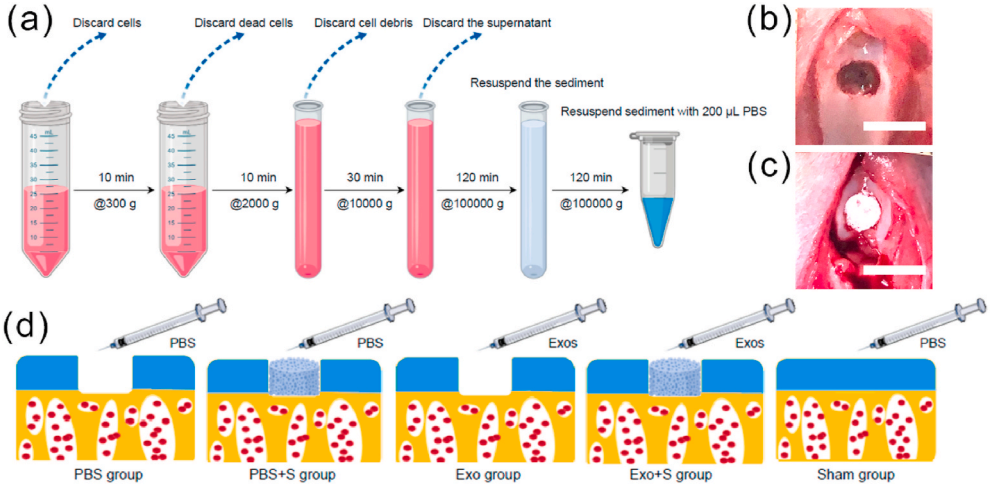

Fig. 2. (a) Extracted exosomes by differential ultracentrifugation. (b) Osteochondral defects model. Scale bar = 5 mm. (c) The ACECM scaffold was implanted into the defect site. (d) Groups used in the osteochondral defects repair experiments.

free medium containing different concentrations of Exos (0 μg/mL, 5 μg/mL, 15 μg/mL, 25 μg/mL), and a control group without cells was established. After 1 day, 4 days, and 7 days, cell counting kit (CCK)-8 reagent was added to wells in each group according to the manufacturer's instructions. After 2 h, a spectrophotometer (Beckman, DU-640) was used to detect the optical density (OD) of the samples.

2.4.2. Influence of Exos on BMSC migration

The following culture media with different Exo concentrations were prepared: a: 0 μg/mL, b: 5 μg/mL, c: 15 μg/mL, and d: 25 μg/mL. A Transwell chamber was soaked with 600 μL of each of the above 4 kinds of culture media and incubated for 30 min. Then, 100 μL of cell suspension (containing 5×10^4 cells) was placed in the upper chamber and cultured for 12 h. The cells were fixed with paraformaldehyde. The cells in the upper chamber were wiped with a sterile cotton swab. The bottom film of the upper chamber was cut and stained with 0.1% crystal violet staining solution. Cell migration was observed under a microscope.

2.4.3. Effect of Exos on macrophage polarization

Medium containing the M2 macrophage inducer IL-4 (20 ng/mL) was used in the positive control group, medium containing Exos (25 μg/mL) was used in the experimental group, and medium containing an equal volume of PBS was used in the control group. Macrophages were seeded in a 12-well plate with three wells in each group and cultured in the above three media for 24 h. The RT-PCR protocol has been reported in previous research by our group [27]. The M2 macrophage marker CD206 was used as the target gene, and specific primers were used for amplification (forward: 5′-ATGGATGTTGATGGCTACTGG-3′, and reverse: 5′-TTCTGACTCTGGACACTTGC-3′). The housekeeping gene glyceraldehyde-3-phosphate dehydrogenase (GAPDH) was used as an internal reference gene. CD206 gene expression was quantified by RT-PCR using a LightCycler 480 system (Roche Applied Science, Indianapolis, IN, USA).

2.5. In vivo animal experiment

2.5.1. Reparative effect of hWJMSC-Exos combined with ACECM scaffold on osteochondral defects

This study was performed according to a protocol approved by the Institutional Animal Care and Use Committee of PLA General Hospital. Round ACECM scaffold samples with a diameter of 3.5 mm and a thickness of 1.5 mm were sterilized with Co60 for use. Fifty adult New Zealand white rabbits were prepared, and in 40 of them, an osteochondral defect with a diameter of 3.5 mm and a depth of 1.5 mm was established in the femoral trochlea (Fig. 2b). Then, the rabbits were randomly divided into 4 groups, with 10 rabbits in each group: the PBS group, the PBS + S group, the Exo group and the Exo + S group. The remaining 10 rabbits were assigned to the sham group (PBS intra-articular injection + sham operation), in which the joint capsule was incised, the patella was immediately reset after dislocation, and then the joint capsule was sutured. In the PBS + S and Exo + S groups, an ACECM scaffold was implanted in the osteochondral defect (Fig. 2c). Animals in the PBS, PBS + S and sham groups received an injection of 200 μL of PBS in the knee joint cavity. Animals in the Exo and Exo + S groups were injected with an equal volume of hWJMSC-Exo suspension at a concentration of 25 μg/mL. Subsequently, injections were administered once every 7 days for a total of 5 injections. The rabbits were allowed to move and eat freely after the operation. The experimental groups are shown in Fig. 2d. The rabbits were euthanized 3 or 6 months after the operation, and the knee joints were collected for the further testing.

2.5.2. Regulatory effect of Exos on the articular cavity microenvironment

Sixteen Sprague-Dawley (SD) rats were randomly divided into a 10-day group and a 20-day group, with 8 rats in each group. Under aseptic conditions, a 2.0-mm-diameter trephine was used to generate an osteochondral defect with a depth of approximately 1 mm in the femoral trochlea of the left leg until there was slight bleeding. The patella was repositioned, and the soft tissue and skin were sutured. The rats received an injection of 50 μL of PBS or an equal volume of 25 μg/mL hWJMSC-Exo suspension in the left knee joint cavity, and the injections were repeated every 7 days thereafter. The rats were allowed to move and eat freely after the operation. At 10 and 20 days after the operation, half of the rats in each group were sacrificed, and the distal femur and joint synovium were collected. The levels of inflammation and macrophage polarization were assessed by immunohistochemical staining (IL-1, IL-10 and TNF-α) and immunofluorescence staining (CD206, CD68, and CD86). The migration of endogenous stem cells was assessed by immunofluorescence staining (CD73 and CD105). Image-Pro Plus 6.0 (Media Cybernetics, USA) was used for quantitative/semiquantitative analysis of the results.

2.6. Macroscopic assessment

All scoring was performed by 3 independent individuals who were blinded to the group assignments. The International Cartilage Repair Society (ICRS) macroscopic evaluation criteria for cartilage repair were used for scoring [28]. The scoring items included the degree of defect repair, the degree of integration with surrounding tissues, the macroscopic performance and the overall macroscopic score.

2.7. Imaging evaluation

2.7.1. Micro-magnetic resonance imaging (micro-MRI)

All rabbit knee joints were scanned by high-resolution animal MRI (7.0-T MRI) (Bruker, BioSpec 70/20 USR) using a T1-weighted imaging (T1WI) sequence. All imaging data were scored by imaging professionals with reference to the Whole-Organ Magnetic Resonance Imaging Score (WORMS) for independent blind scoring [29]. The contents of the evaluation included cartilage, bone marrow abnormalities, bone cysts, bone wear and osteophytes.

2.7.2. Microcomputed tomography (micro-CT)

Micro-CT (GE) was used to evaluate the regeneration of subchondral bone in the knee joint at 3 and 6 months after surgery. The volume of interest was selected in the subchondral bone of each defect area (diameter = 3.5 mm, thickness = 1 mm). Subchondral bone regeneration was estimated based on the bone volume fraction (BVF) and trabecular bone thickness (Tb.Th) per tissue volume.

2.8. Histomorphological evaluation

After the sample was fixed, decalcified, and dehydrated, it was embedded in paraffin and sectioned at 5 μm. Sections were stained with hematoxylin and eosin (H&E) and safranin O-fast green according to the manufacturer's instructions. According to previous studies [30,31], sections were also subjected to type II collagen immunohistochemistry (collagen II antibody, Novus, NB600-844). Images of sections in each group were captured with a bright-field microscope (Nikon, Japan) at 100 × magnification. The staining results of the above sections were scored blindly by three researchers in related fields according to the histomorphology scoring system [32] to evaluate the effects on the repair of cartilage and subchondral bone in each group.

2.9. Biomechanical testing

Special equipment (Bose, 5100) was used to test the mechanical properties of the repaired tissue at 3 and 6 months after surgery. According to Hooke's law, within the elastic limit of an object, stress and strain become proportional, and its proportional coefficient is called Young's modulus (denoted as E). Young's modulus is calculated using the following formula: $E=(F \cdot L)/(S \cdot \Delta L)$, where F is the applied pressure, S is the indenter area, L is the total cartilage thickness (default is 1 mm),

and ΔL is the deformation variable.

2.10. Biochemical assay

According to the manufacturer's instructions, a hydroxyproline test kit (Nanjing Jiancheng, A030-2-1) was used to detect the hydroxyproline content of new cartilage. According to the content of hydroxyproline in collagen (13.4%), the collagen content in the repaired tissue was calculated.

2.11. Exos small RNA sequencing and data analysis

2.11.1. ExoRNA library construction and sequencing

The miRNeasy® Mini kit (Qiagen, cat. no. 217004) was used to extract exosomal RNA from the cell culture supernatant. To construct a small RNA library, the input amount of each sample was 1–500 ng, and the index sequence was added. A UMI library building kit (QIAseq miRNA Library Kit, Qiagen, Frederick, MD), which can add a unique UMI sequence to each miRNA, was used. Index-labeled samples were clustered in the acBot Cluster Generation system using TruSeq PE Cluster Kitv3-cBot-HS (Illumina, San Diego, CA, USA), and then paired-end sequencing was performed on the Illumina HiSeq platform.

2.11.2. miRNA analysis

(1) miRNA analysis and target gene prediction

Through Bowtie, clean reads were compared with the Silva, GtRNAdb, Rfam and Repbase databases to filter out ribosomal RNA (rRNA), transfer RNA (tRNA), small nuclear RNA (snRNA), small nucleolar RNA (snoRNA) and other noncoding RNA (ncRNA) and repetitive sequences. The remaining reads were compared with known miRNAs in the miRbase database (v22) to quantify their expression. miRDeep2 software was used to compare reads that did not match known miRNAs with the human genome (GRCh38) to predict new miRNAs. The read number of each miRNA was obtained by comparison and correction. For the top 50 highly abundant miRNAs with transcripts per million (TPM) expression, the multiMiR package (R language) was used to predict miRNA target genes.

(2) Enrichment analysis of Gene Ontology (GO) and Kyoto Encyclopedia of Genes and Genomes (KEGG) pathways

The clusterProfiler package was used to perform functional annotation and enrichment analysis of KEGG and GO data for the top 50 high-abundance miRNA target genes. For the three major categories in the GO database (biological processes, cell components, and molecular functions), as well as the KEGG pathways, the 20 most significant terms/pathways are displayed.

2.12. Statistical analysis

SPSS 18.0 (SPSS, Inc., Chicago, IL, USA) was used to analyze the data. Values are expressed as the mean ± standard error. One-way analysis of variance was used for data with a homogeneous variance, and then the Bonferroni post hoc test was performed. The rank-sum test was used for data with a nonhomogeneous variance to identify significant differences between groups. $P < 0.05$ was considered to indicate a statistically significant difference.

3. Results

3.1. hWJMSCs express MSC-specific markers and are capable of multilineage differentiation

Wharton's jelly wraps around the umbilical blood vessels and gives the appearance of a viscous jelly (Fig. 3a). The cultured hWJMSCs showed a uniform, slender, spindle shape and a typical spiral arrangement under the microscope (Fig. 3b). There were many cells in the division pattern, and the cells grew vigorously.

The flow cytometry results of hWJMSCs showed that the cells expressed the MSC surface markers CD73 (98.4%), CD90 (99.4%), and CD105 (100%) (positive rates ≥ 95%) and did not express the hematopoietic cell markers CD34 (0.036%) and CD45 (0.063%) (positive rates ≤ 2%) (Fig. 3f). These data show that hWJMSCs isolated and cultured without digestive enzymes are homogeneous, without hematopoietic cells and endothelial cells, and have good MSC characteristics.

After 21 days of culture in osteogenic induction medium, alizarin red staining showed a large amount of matrix calcification with calcium nodule formation (Fig. 3c), proving that the hWJMSCs were capable of osteogenic differentiation. After 21 days of culture in adipogenic induction medium, a large number of round, red-stained lipid droplets were observed by oil red O staining (Fig. 3d). After 21 days of culture in chondrogenic induction medium, alcian blue staining was positive (Fig. 3e), indicating that the 3D cell pellets were rich in proteoglycans. The above experimental results confirm that hWJMSCs are capable of multilineage differentiation.

3.2. hWJMSC-Exos have the morphological characteristics of Exos and express specific markers of Exos

TEM observation showed that the Exos appeared as discs with a diameter of approximately 100 nm (Fig. 3g). The NTA results showed that the peak particle size was 135 nm (Fig. 3h). The WB results confirmed that the hWJMSC-Exos highly expressed the Exo protein markers CD9, TSG101 and CD63 but did not express the Exo-negative protein marker calnexin (Fig. 3i). CD63 is a glycosylated protein, and its varying glycosylation levels result in a diffuse band.

The above experimental results prove that the Exos isolated from the culture supernatant of hWJMSCs have a typical morphology, good uniformity, and characteristics of Exos.

3.3. ACECM scaffold surface is loose and porous, has a vertically oriented structure, and has good cytocompatibility

ACECM looks like a loose porous sponge to the naked eye (Fig. 4a). SEM observation of a cross-section of the scaffold showed that the pore diameter was approximately 200 μm (Fig. 4b), and observation of a longitudinal section of the scaffold showed an obvious longitudinally aligned structure, similar to the structure of natural articular cartilage cells (Fig. 4c). The SEM results obtained 4 days after the cells were seeded on the scaffold showed that the cells had aggregated and adhered to the scaffold (Fig. 4d).

The results of confocal laser observation after BMSCs were seeded on the ACECM scaffold (Fig. 4e–g) showed slight cell growth on the first day; however, the cells had aggregated into clusters by the fourth day and connected into sheets by the seventh day. Live cells (green) accounted for the vast majority of cells, and only a few cells died (red), confirming that the scaffold had good cytocompatibility.

3.4. Exos can promote BMSC and chondrocyte proliferation, BMSC migration and macrophage polarization toward the M2 phenotype in vitro

The Transwell assay results showed that Exos can promote the migration of BMSCs in a dose-dependent manner (Fig. 5a). The results of the statistical analysis showed that 25 μg/mL Exos had the strongest effect (Fig. 5b).

At 1 day, compared with PBS, Exos did not promote the proliferation of BMSCs or chondrocytes (Fig. 5c and d). However, at 4 and 7 days, Exos significantly promoted the proliferation of BMSCs and chondrocytes. The effect of Exos on the proliferation of chondrocytes was

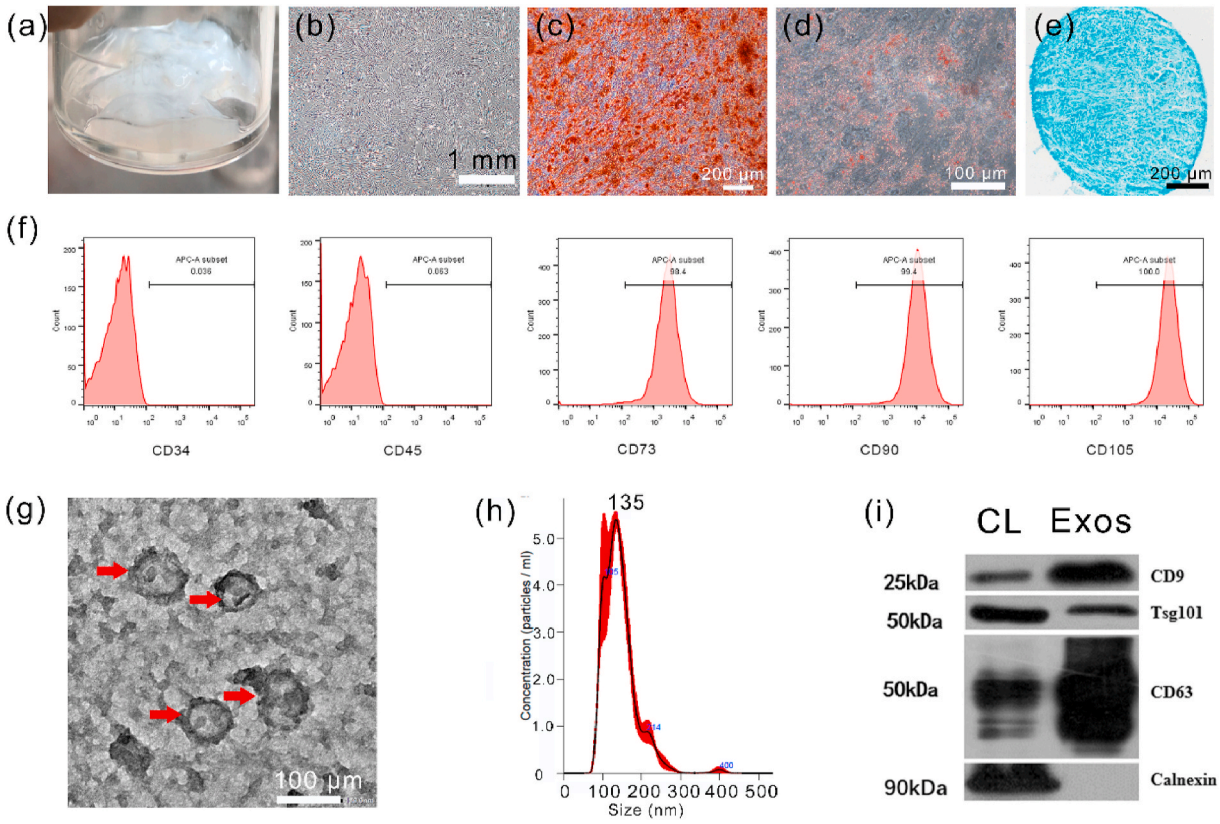

Fig. 3. (a) Wharton's jelly stripped from the umbilical cord. (b) P3-generation hWJMSCs morphology under an optical inverted microscope. (c) Osteogenic differentiation of hWJMSCs stained with alizarin red (× 100). (d) hWJMSCs differentiated into fat and stained with oil red O (× 200). (e) hWJMSCs differentiated into cartilage and stained with alcian blue (× 40). (f) Flow cytometry showed that hWJMSCs highly expressed CD73, CD90, and CD105 (both ≥95%) but did not express CD34 and CD45 (both ≤2%). (g) TEM shows that Exos have the shape of a disc with a diameter of approximately 100 nm (Exos shown by the red arrowhead). (h) NTA shows the particle size distribution of Exos. (i) WB results for the Exo markers CD9, TSG101, and CD63 and the negative marker Calnexin. CL is a positive control (cell lysate). (For interpretation of the references to color in this figure legend, the reader is referred to the Web version of this article.)

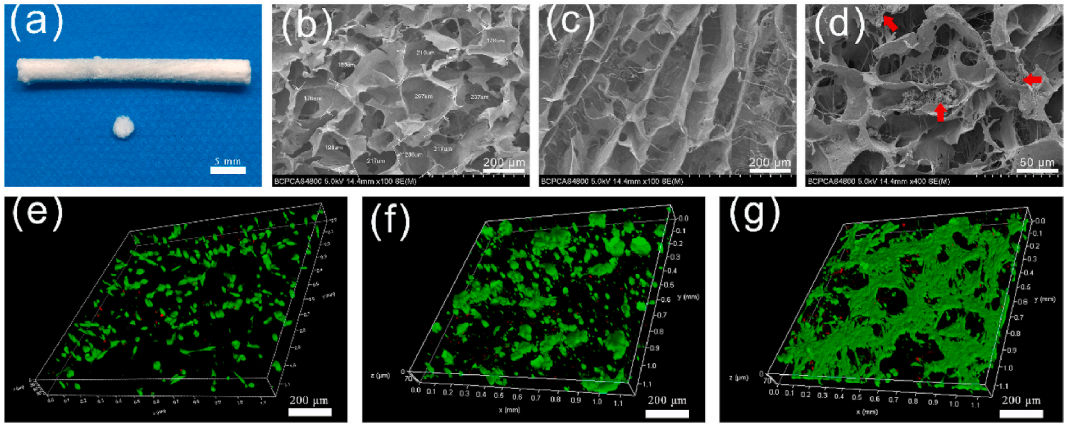

Fig. 4. (a) Macroscopic view of the ACECM scaffold. (b) SEM results of the cross-section of the ACECM scaffold. (c) SEM results for a longitudinal section of the ACECM scaffold. (d) SEM results for BMSCs planted on the ACECM scaffold for 4 days (the red arrowhead indicates the clustered cells). (e–g) Confocal laser observation of live/dead-stained BMSCs planted on the ACECM scaffold for 1, 4, and 7 days (green indicates live cells, and red indicates dead cells). (For interpretation of the references to color in this figure legend, the reader is referred to the Web version of this article.)

obviously dose-dependent, but when BMSCs were cultured for 7 days, there was no significant difference between the Exos concentration of 15 μg/mL and 25 μg/mL in promoting proliferation.

The RT-PCR results showed that Exos can significantly promote CD206 gene expression in macrophages compared to PBS, which means that Exos promote the polarization of macrophages toward the M2 phenotype.

3.5. hWJMSC-Exos combined with ACECM scaffold promote articular cartilage regeneration

(1) Macroscopic evaluation

The macroscopic results of cartilage regeneration at 3 and 6 months after surgery are shown in Fig. 6a. Three months after the operation,

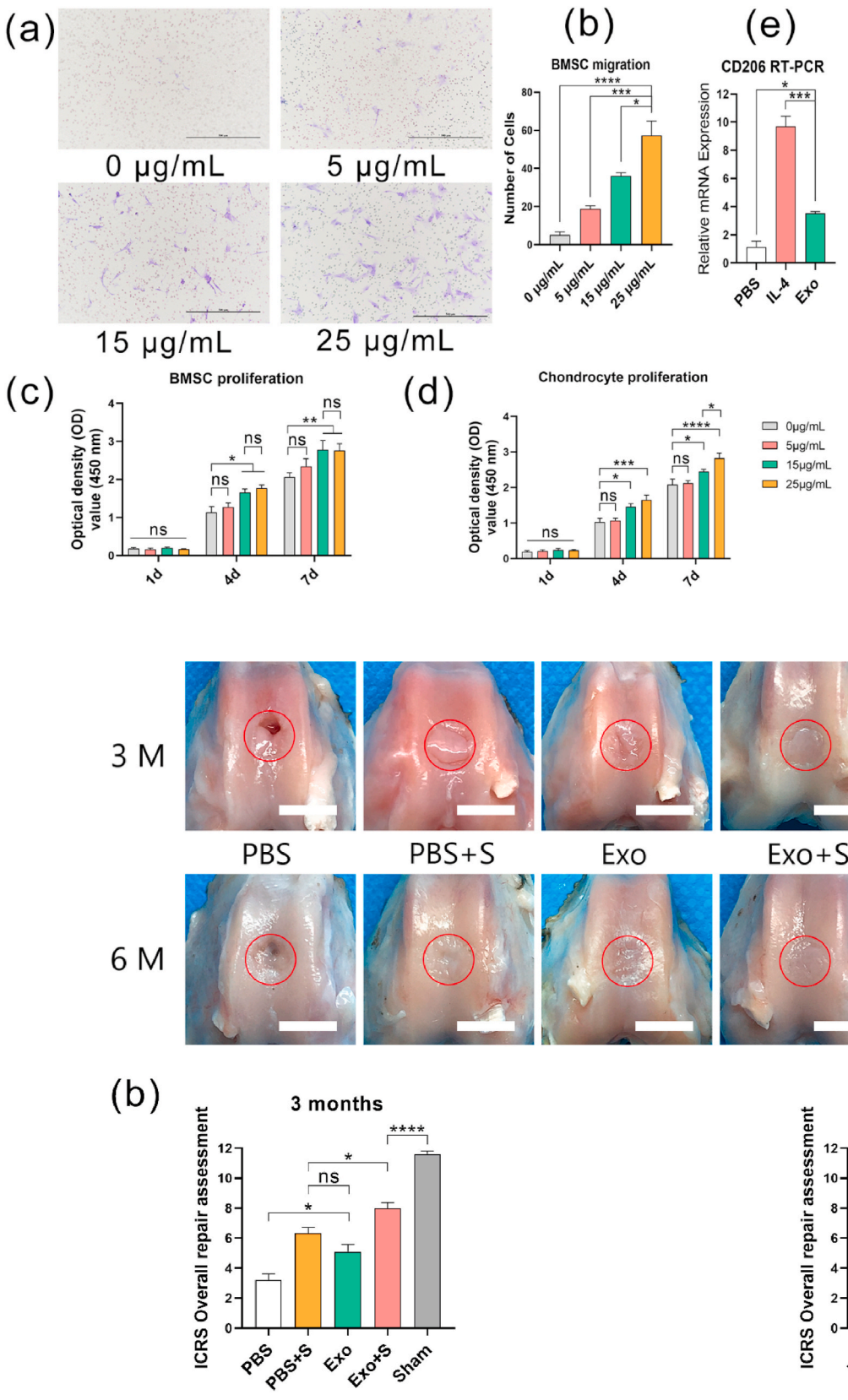

Fig. 5. (a) Effects of different concentrations of Exos on the migration of BMSCs in vitro (purple shows the cells). Scale bar = 500 μm. (b) Effects of Exos on the migration of BMSCs in vitro (Transwell method). (c) Effects of Exos on the proliferation of BMSCs in vitro (CCK-8 method). (d) Effects of Exos on the proliferation of chondrocytes in vitro (CCK-8 method). (e) The effect of Exos on macrophage polarization in vitro (RT-PCR). (*P < 0.05, **P < 0.01, ***P < 0.005, ****P < 0.001). (For interpretation of the references to color in this figure legend, the reader is referred to the Web version of this article.)

Fig. 6. (a) Macroscopic results for new cartilage. The red circles show the locations of the defects. Scale bar = 5 mm. (b) ICRS cartilage repair macroscopic score. (*P < 0.05, **P < 0.01, ***P < 0.005, ****P < 0.001). (For interpretation of the references to color in this figure legend, the reader is referred to the Web version of this article.)

repaired tissue was visible at the defect site in all groups, but in the PBS group, only a small amount of fibrous tissue-like tissue with a rough surface and local defects with a depth exceeding the cartilage thickness were visible. The height of the repaired tissue in the PBS + S and Exo groups was significantly lower than that of the surrounding normal cartilage, the surface was uneven, and the defect boundary was still obvious. The repaired tissue in the Exo + S group essentially filled the defect area, but the boundary was still visible. At 6 months, the level of repaired tissue was lower than that of the surrounding normal cartilage in the PBS and Exo groups but essentially the same height as the surrounding normal cartilage in the PBS + S and Exo + S groups. In the Exo + S group, a smooth surface and no obvious boundary with the surrounding normal cartilage were observed, which was significantly better than result in the PBS + S group. The ICRS cartilage repair macroscopic score (Fig. 6b) showed significantly better repair in the Exo + S group than in the other groups at 3 and 6 months.

(2) Imaging evaluation

T1 micro-MRI (Fig. 7a) showed that the osteochondral defects in all groups exhibited cartilage edge continuity interruption at 3 months, and the repaired tissue showed signals different from those of mature cartilage. The subchondral bone in the PBS group was significantly collapsed, and the defect reached the bone marrow cavity. The defects were smallest in the Exo + S group, indicating the best reparative effect. At 6 months, the cartilage defects in all groups had been filled with repaired tissue, but only the repaired tissue in the Exo + S group showed signals close to those of normal cartilage. The 3- and 6-month MRI WORMS results (Fig. 7c) also showed significantly better results in the Exo + S group than in the other groups. The micro-CT results (Fig. 7b) showed that the surface of the subchondral bone in the Exo + S group was smooth and was similar to that in the sham group at 6 months. The subchondral bone in the other groups was not smooth and showed different degrees of bone loss. The subchondral bone in the PBS group was significantly collapsed. BVF analysis (Fig. 7d) also confirmed this point. At 6 months, only the Exo + S and sham groups showed results that were not significantly different. These findings indicate that the best subchondral bone reconstruction was achieved in the Exo + S group, with a level close to that of the normal cartilage. The results of Tb.Th analysis by CT (Fig. 7e) showed that at 6 months, except for the PBS group, none of the other groups showed significant differences from the sham group.

(3) Histomorphological evaluation

Histomorphological staining can best illustrate the nature of repaired tissue. Generally, as time progresses, osteochondral defects are gradually filled with repaired tissue. The results of H&E staining (Fig. 8a) were similar to the results of the macroscopic evaluation. There was still a gap between the repaired tissue and normal cartilage in the Exo + S group at 3 months, but the repaired tissue was almost completely fused with the normal cartilage at 6 months. The cells in the repaired tissue were clearly arranged in a vertical column (Fig. 8b), similar to those in normal cartilage, and the subchondral bone was well reconstructed. In the PBS group, the subchondral bone collapsed, and the repaired tissue appeared as disorderly, loose, fibrous tissue covering the defect surface. In contrast, there was no obvious subchondral bone collapse in the PBS + S or Exo group. However, the surface of the new cartilage in the PBS + S and Exo groups was not smooth, and flocculent fibrous tissue was visible.

Safranin O can be used to stain polysaccharides in cartilage red. The deeper the red color is, the higher the polysaccharide content. Fast green can be used to stain bone tissue green (Fig. 8c). The repaired tissue in the Exo + S group showed red staining in only the lower half of the tissue at 3 months, while all of the tissue was stained red at 6 months, indicating that as the repair progressed, the polysaccharide content of the new cartilage gradually increased. The little repaired tissue present in the PBS group contained almost no polysaccharides, and the polysaccharide content in the PBS + S and Exo groups was higher than that in the PBS group.

The level of type II collagen in the repaired tissue was verified by immunohistochemical staining (Fig. 8d). At 3 months, the new cartilage in the Exo + S group showed obvious coloration, which was significantly better than that in the other three groups, but the staining of the new cartilage was lighter than that of the surrounding normal cartilage, indicating that its type II collagen content was still lower than that of normal cartilage. At 6 months, the immunohistochemical staining of the new cartilage in the Exo + S group showed no significant difference from that of the surrounding normal cartilage, and the surface of the new cartilage was smooth. The type II collagen content in the PBS + S and Exo groups was lower than that in the Exo + S group, and the least collagen was observed in the PBS group, with fibrous, flocculent tissue.

The histomorphology scores were consistent with the staining results. The cartilage score (Fig. 8e) in the Exo + S group was significantly superior to that in the other groups at both 3 and 6 months. The subchondral bone score (Fig. 8f) in the Exo + S group was not significantly different from that in the PBS + S group at 6 months, but it was significantly better than that in the PBS and Exo groups.

(4) Biomechanical evaluation

Biomechanical testing can be used to evaluate the mechanical properties of new cartilage. Under normal circumstances, the Young's modulus of hyaline cartilage is higher than that of fibrocartilage. According to the results (Fig. 8g), the Young's modulus in the Exo + S group was significantly higher than that in the other groups at 3 months but still significantly lower than that in the sham group. At 6 months, although the Young's modulus in the Exo + S group was still lower than that in the sham group, there was no significant difference between the two groups.

(5) Biochemical assay

At 3 months, the collagen content (Fig. 8h) of the repaired tissue in the Exo + S group was significantly higher than that in the other groups but lower than that of normal cartilage. At 6 months, there was no significant difference between the Exo + S and sham groups, which was consistent with the results of type II collagen immunohistochemical staining.

3.6. hWJMSC-Exos regulate joint cavity inflammation by inducing macrophage polarization toward the M2 phenotype

The microenvironment of the joint cavity plays an important role in cartilage regeneration. A large number of studies have confirmed that MSCs can regulate the inflammatory response of the microenvironment [33]. To verify whether this effect is mediated by Exos, we injected hWJMSC-Exos into the knee joint cavity in a rat osteochondral defect model. Immunohistochemical staining for the proinflammatory cytokines TNF-α and IL-1 and the anti-inflammatory cytokine IL-10 in the joint synovium and the repaired tissue of the defect (Fig. 9a) can reflect the level of inflammation. Compared with the PBS group, the Exo group showed no significant difference in the expression level of IL-1 or TNF-α (Fig. 9c and d), but the expression level of IL-10 was significantly increased (Fig. 9b), indicating a lower level of inflammation.

To further explore the mechanism by which Exos regulate inflammation, we performed immunofluorescence staining for CD68, CD86, and CD206 (Fig. 10a and b), specific markers of all macrophages, M1-type macrophages, and M2-type macrophages, respectively, in the joint synovium, to evaluate the effect of hWJMSC-Exos on macrophage polarization. The results showed that at 10 and 20 days, the proportion of both M2-type macrophages (Fig. 10c) and all macrophages (Fig. 10d)

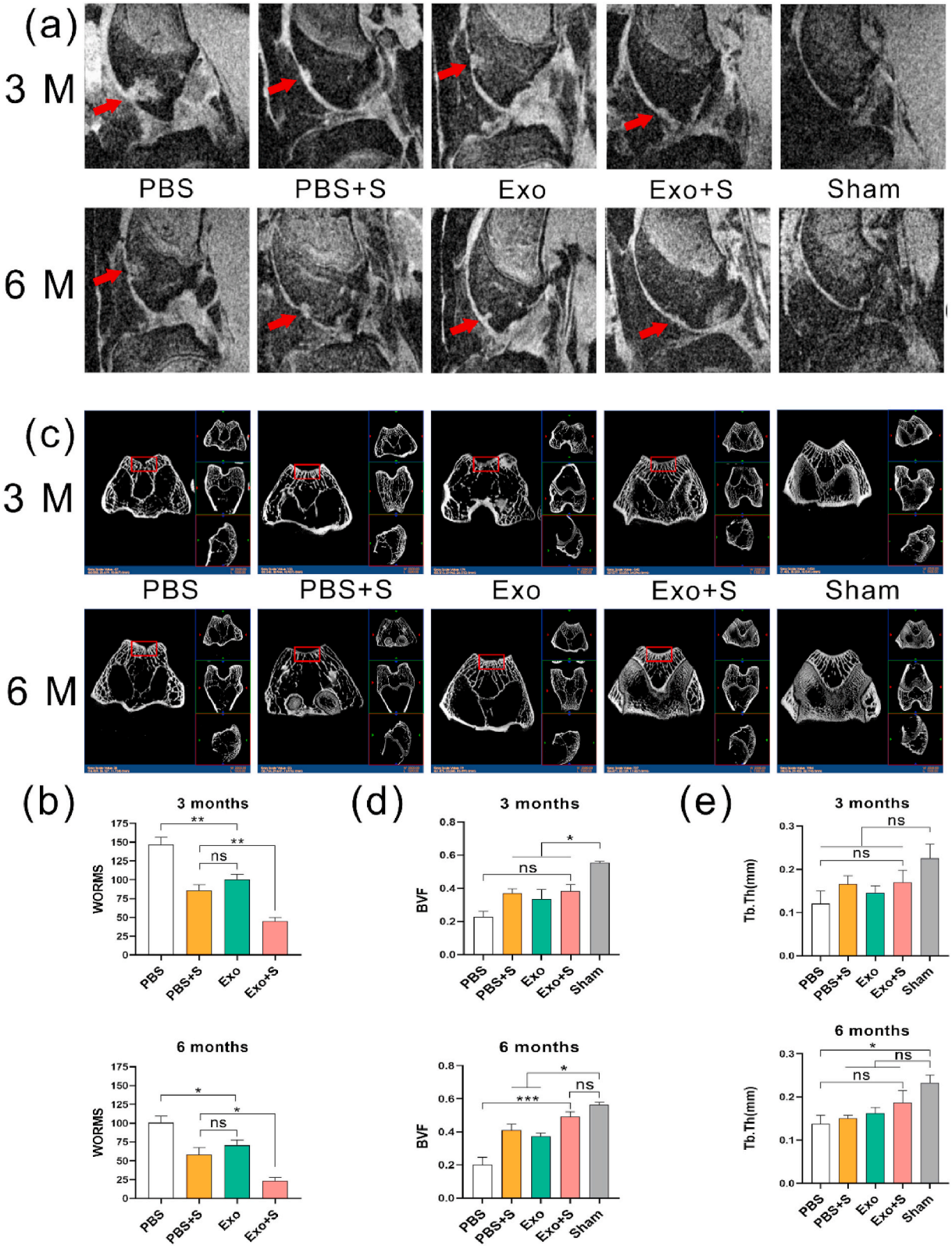

Fig. 7. (a) Micro-MRI findings. The red arrowheads show the locations of the defects. (b) MRI WORMS score results. (c) Micro-CT findings, the red rectangles show the subchondral bone at the defect sites. (d–e) Micro-CT BVF analysis and Tb.Th analysis results. (*P < 0.05, **P < 0.01, ***P < 0.005, ****P < 0.001). (For interpretation of the references to color in this figure legend, the reader is referred to the Web version of this article.)

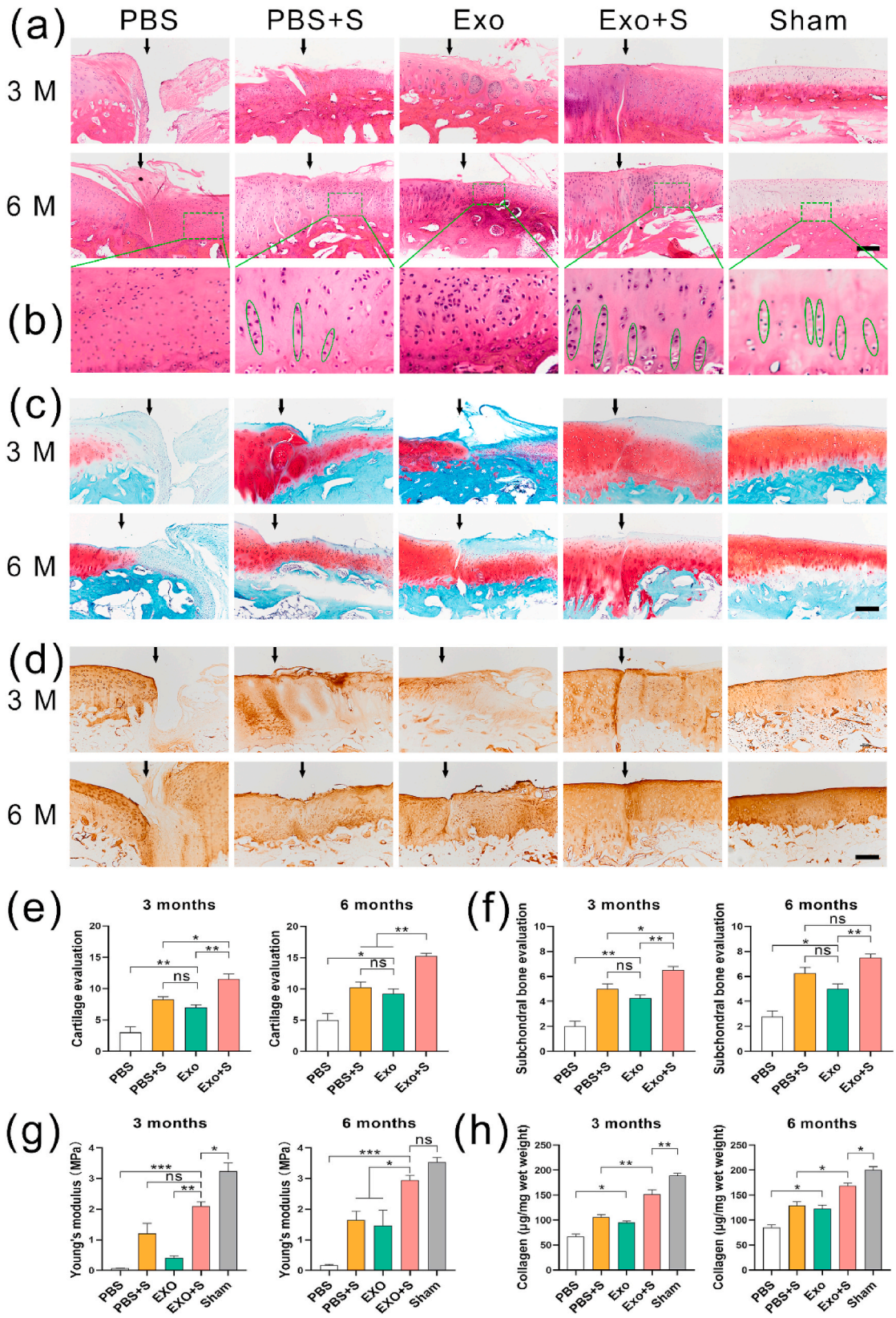

Fig. 8. (a) HE staining results. The black arrow indicates the defect boundary. The left side of the arrow is normal cartilage, and the right side of the arrow is repaired tissue. Scale bar = 100 μm. (b) Safranin O-fast green staining result. Scale bar = 100 μm. (c) Type II collagen immunohistochemical staining results. Scale bar = 100 μm. (d) Histomorphology score of the repaired tissue (cartilage). (e) Histomorphology score of the repaired tissue (subchondral bone). (f) Young's modulus of the repaired tissue. (g) The collagen content of the repaired tissue. (*P < 0.05, **P < 0.01, ***P < 0.005, ****P < 0.001). (For interpretation of the references to color in this figure legend, the reader is referred to the Web version of this article.)

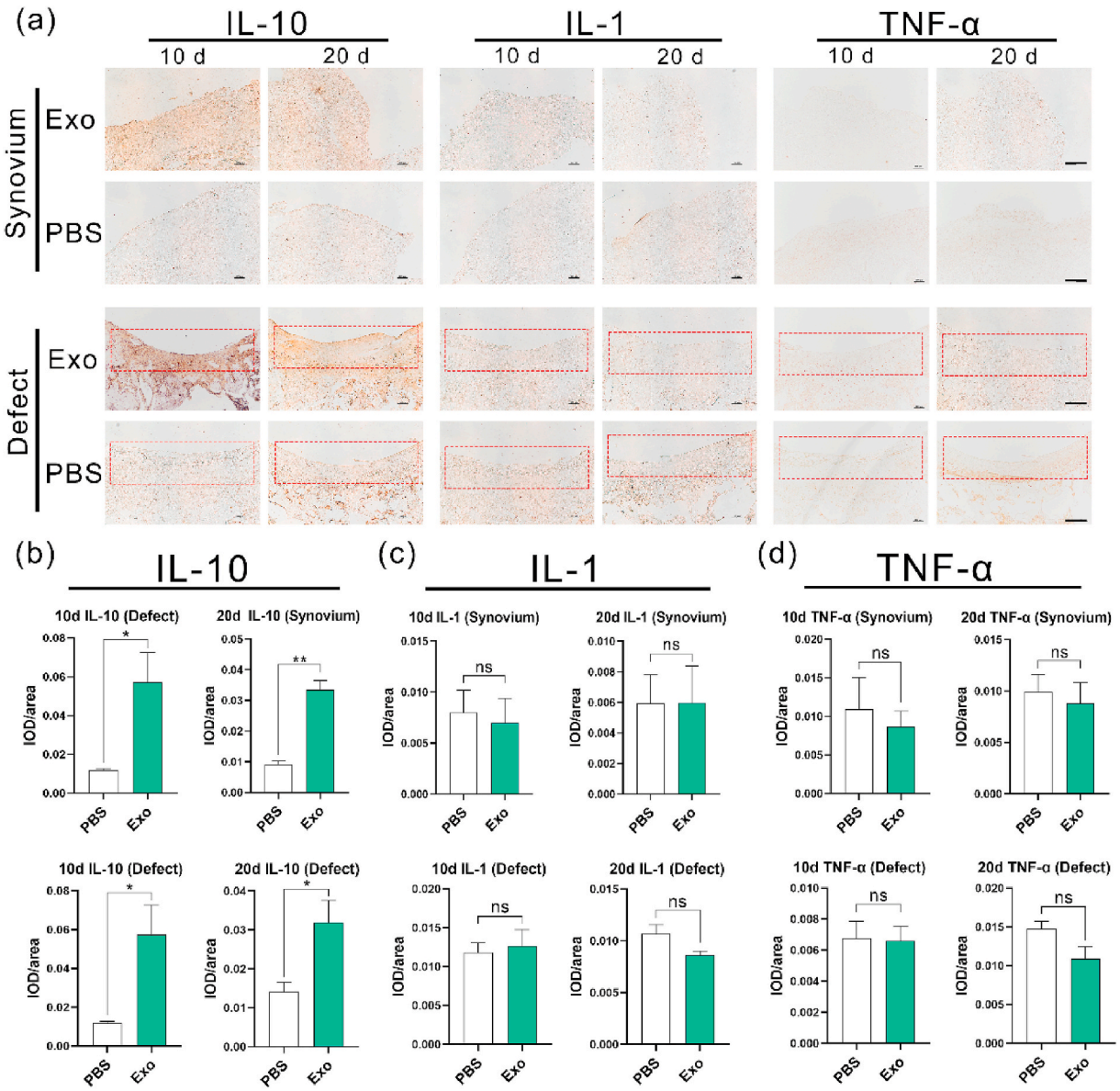

Fig. 9. (a) Immunohistochemical staining (IL-10, IL-1, TNF-α) for synovium and the osteochondral defects in rats at 10 and 20 days after surgery, the red rectangles show the repaired tissue, scale bar = 200 μm. (b–d) Semi-quantitative results of immunohistochemical staining for IL-10, IL-1 and TNF-α. (*P < 0.05, **P < 0.01, ***P < 0.005, ****P < 0.001). (For interpretation of the references to color in this figure legend, the reader is referred to the Web version of this article.)

was significantly increased in the Exo group. In contrast, the proportion of M1-type macrophages was significantly reduced in the Exo group (Fig. 10e). The above results confirm that hWJMSC-Exos promote the infiltration of macrophages in vivo and promote the polarization of macrophages toward the M2 phenotype.

This study confirmed that hWJMSC-Exos can promote the migration of BMSCs in vitro. Immunofluorescence staining for the MSC-specific markers CD73 and CD105 (Fig. 11a and b) was used to verify whether Exos can promote the migration of endogenous stem cells to cartilage defects in vivo. However, the staining results showed that there were fewer MSCs in the cartilage defect in the Exo and PBS groups, and most of them were concentrated at the edge of the defect. Additionally, statistical analysis (Fig. 11c) showed that the Exo group had more MSCs than the PBS group, but there was no significant difference.

3.7. hWJMSC-Exos miRNA sequencing and bioinformatic analysis

Exos can posttranscriptionally regulate coding genes through miRNAs, thereby affecting the biological activities of recipient cells. Fig. 10a shows the top 50 high-abundance miRNAs in hWJMSC-Exos according to the total read count.

Interestingly, hWJMSC-Exos were rich in miR148a and miR29b (Fig. 12a). miR148a has been confirmed to promote cartilage regeneration by inhibiting the differentiation of chondrocytes into a hypertrophic phenotype and promoting the secretion of proteoglycans and collagen (especially type II collagen) [34]. miR29b plays an important regulatory role in the differentiation of BMSCs into chondrocytes and can significantly inhibit the expression of type I and type III collagen [35], thereby significantly affecting the composition of the new cartilage ECM. The expression levels of miRNA199a, miRNA125b, miRNA221, and miRNA92a have been confirmed to be decreased in previous OA pathology studies [36–39]. The high content of these miRNAs in hWJMSC-Exos suggests the potential inhibitory effect of hWJMSC-Exos on OA. In addition, among the top 50 miRNAs, many potentially beneficial miRNAs have been discovered. Although there is no direct evidence that these miRNAs can promote cartilage regeneration, studies

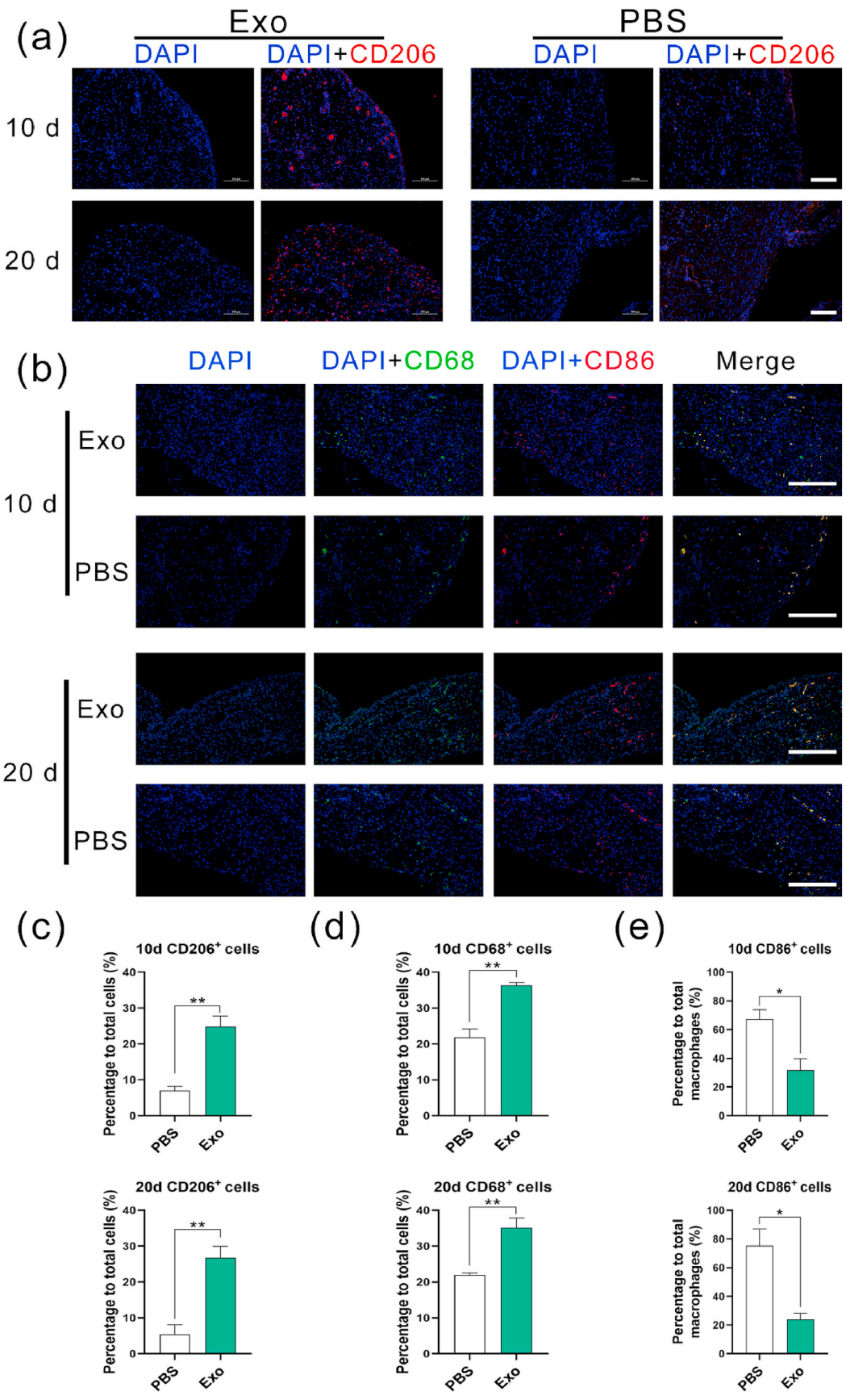

Fig. 10. (a) DAPI and CD206 immunofluorescence staining of the synovium in rats at 10 days and 20 days after surgery, blue fluorescence are the nucleus, red fluorescence are the CD206 positive cells, scale bar = 100 μm. (b) DAPI, CD68和CD86 immunofluorescence staining of the synovium in rats at 10 days and 20 days after surgery, blue fluorescence are the nucleus, green fluorescence are the CD68 positive cells, red fluorescence are the CD86 positive cells, scale bar = 100 μm. (c) The rate of CD206 positive cells in the synovium. (d) The rate of CD68 positive cells in the synovium. (e) The proportion of CD86 positive cells to total macrophages. (*P < 0.05, **P < 0.01, ***P < 0.005, ****P < 0.001). (For interpretation of the references to color in this figure legend, the reader is referred to the Web version of this article.)

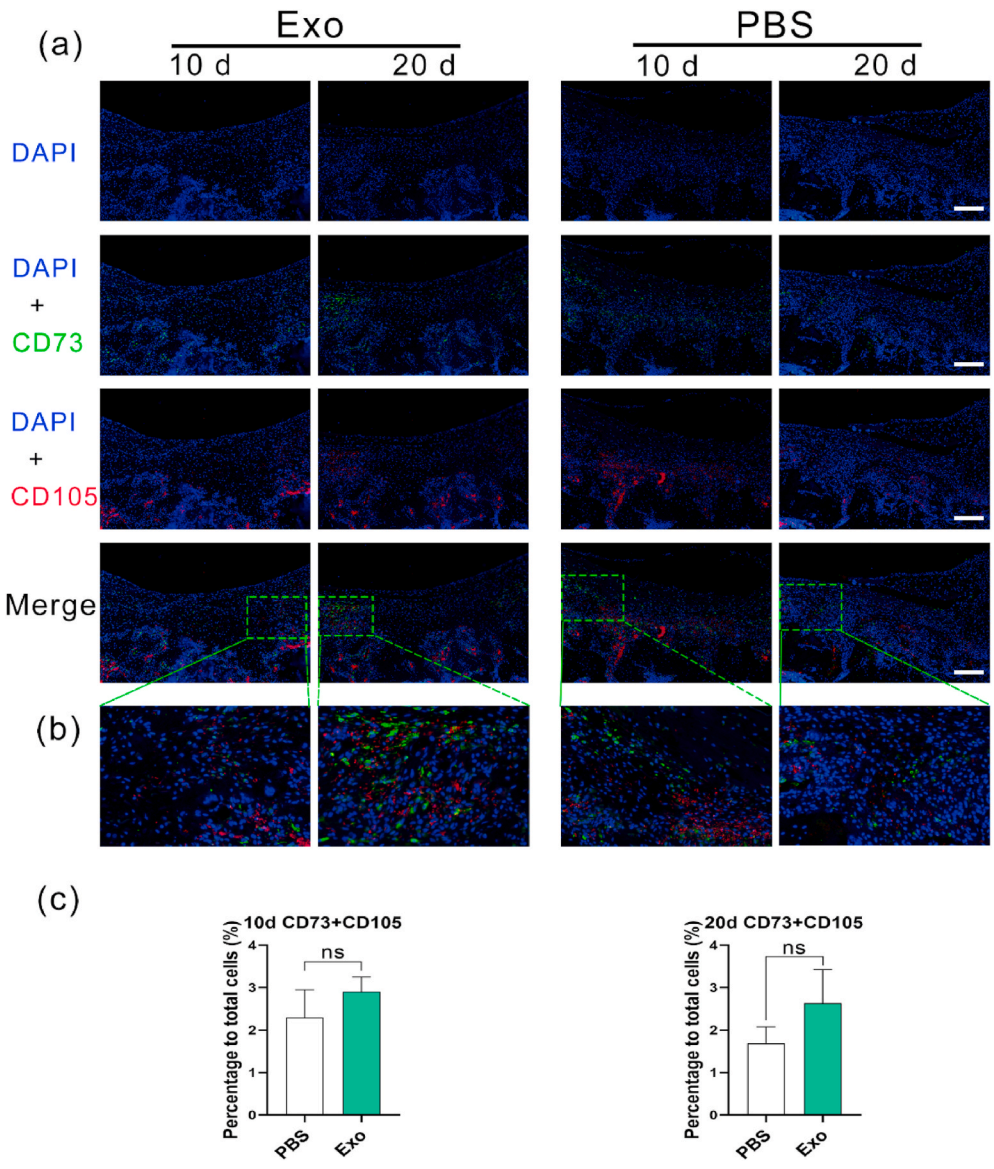

Fig. 11. (a) The immunotissue fluorescence staining of the osteochondral defects of rats at 10 days and 20 days after surgery, blue fluorescence are the nucleus, green fluorescence are CD73 positive cells, red fluorescence are CD105 positive cells, scale bar = 100 μm. (b) The enlarged images of the area show by the green rectangles in Fig. 11a. (c) Statistical analysis results of CD73 and CD105 double positive cells. (*P < 0.05, **P < 0.01, ***P < 0.005, ****P < 0.001). (For interpretation of the references to color in this figure legend, the reader is referred to the Web version of this article.)

have found that they can promote the regeneration of other tissues, such as miR155 (liver regeneration) [40], miR382 (liver regeneration) [41], miR43 (intestinal epithelial regeneration) [42], and miR199 (cardiac regeneration) [43].

The preliminary results of this study confirm the beneficial effects of hWJMSC-Exos in promoting the polarization of macrophages toward the M2 phenotype, immune regulation (especially inhibiting the inflammatory response), and stem cell migration. A search of the literature showed that the DKK3 [44], IL4/SDF-1 (CXCL12) [45] and POSTN/CCL2 [46] genes play a regulatory role in the above biological processes. According to the miRNA target gene prediction results, a total of 230 miRNAs in hWJMSC-Exos target the above genes (Supplementary Material 1). Among them, the multiMiR analysis confirmed at least 2 predictions, and 1 experiment verified this targeting relationship for 20 miRNAs (Table 1). These miRNAs may promote osteochondral regeneration through the above biological processes.

In addition, functional enrichment can better determine the dominant pathway controlled by hWJMSC-Exos [47]. KEGG pathway enrichment (Fig. 12b) was dominated by the cancer pathway, the PI3K-Akt signaling pathway and the MAPK signaling pathway. GO analysis (Fig. 12c–e) showed that "positive regulation of transcription from RNA polymerase II promoter" and "negative regulation of transcription from RNA polymerase II promoter" in the biological process component, "cytosol" and "nucleoclass" in the cellular component, and "ATP binding" and "RNA binding" in the molecular function component had the highest significance. In summary, these results indicate a possible contribution of exosomal miRNAs in promoting cartilage regeneration.

4. Discussion

The intra-articular injection of MSCs has been confirmed to promote cartilage regeneration [48]. Due to the advancement of tissue engineering technology, MSC-based regenerative medicine is no longer limited to the direct injection of MSCs into the joint cavity. On the one hand, scaffolds provide the necessary microenvironment and structure for the regeneration process [49–51]. Scaffold materials mainly include artificial polymeric materials and natural biomaterials [52,53]. Among them, biomaterials derived from the ECM have received wide attention because of their good biocompatibility and safety [54]. On the other hand, the safety problem of MSC transplantation has not been resolved. An increasing number of studies have been devoted to the development of "cell-free" tissue-engineered cartilage based on MSCs, and Exos are considered a good substitute for MSCs [55].

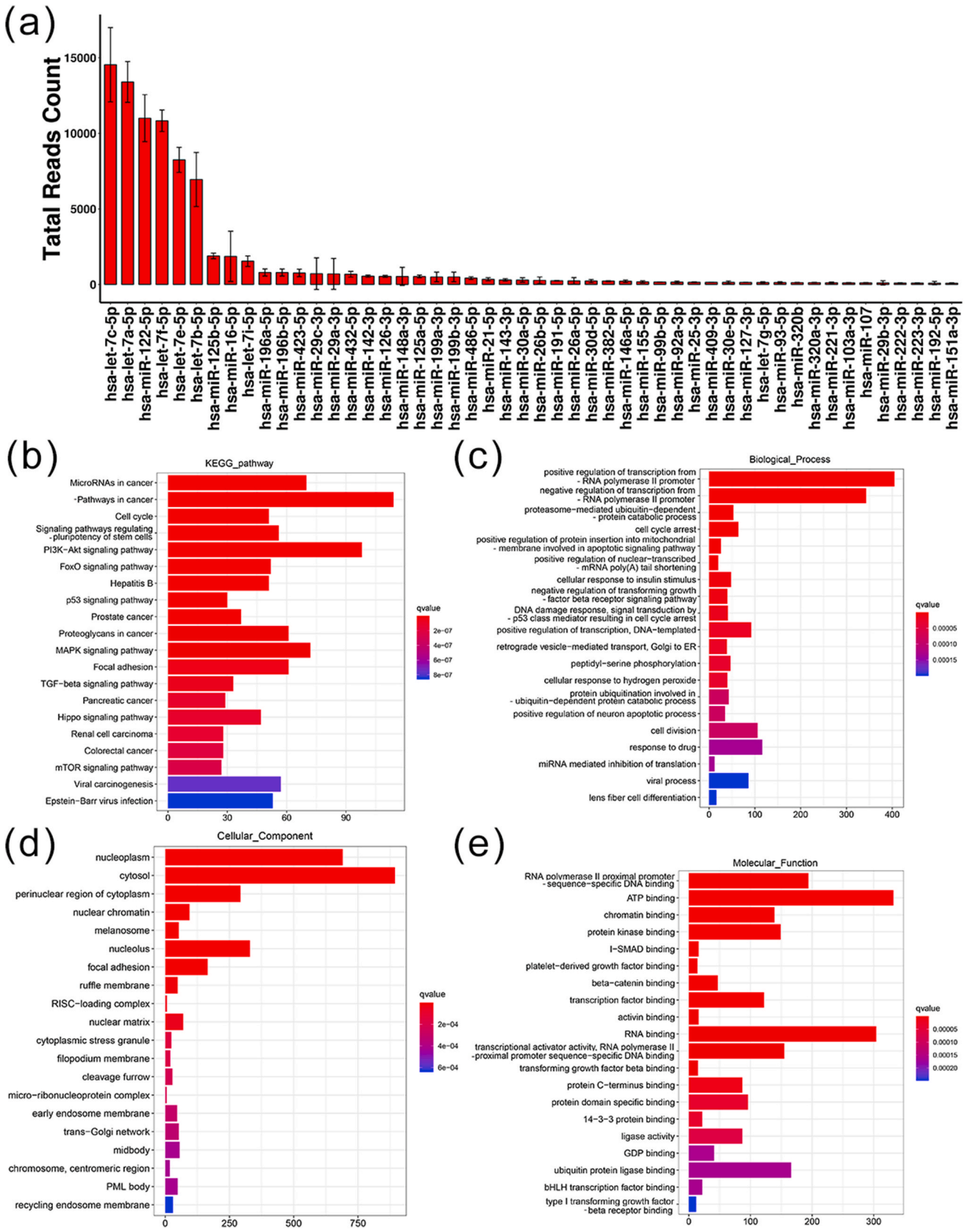

Fig. 12. (a) The top 50 high-abundance miRNAs according to the total read count of hWJMSC-Exo miRNA sequencing. The abscissa represents each miRNA, and the ordinate represents the count values of these miRNAs; (b–e) The target genes of Top50 miRNAs were enriched in KEGG analysis, GO biological process analysis, GO cellular component analysis and GO molecular function analysis (the first 20 results were plotted). The abscissa represents the number of genes annotated in the pathway, the ordinate represents the pathway, the color of the column represents the q value, and $q < 0.05$ was significant. (For interpretation of the references to color in this figure legend, the reader is referred to the Web version of this article.)

Table 1
The targeting relationship between exosomal miRNAs and genes.

Target Gene	miRNA
DKK3	hsa-miR-92b-3p,hsa-miR-32-5p,hsa-let-7b-5p,hsa-miR-19a-3p,hsa-miR-19b-3p
CXCL12	hsa-miR-23a-3p,hsa-miR-221-3p,hsa-miR-23b-3p,hsa-miR-141-3p, hsa-miR-144-3p,hsa-miR-200a-3p,hsa-miR-454-3p,hsa-miR-23c,hsa-miR-320b
CCL2	hsa-miR-374a-5p,hsa-miR-495-3p,hsa-miR-323a-3p
POSTN	hsa-miR-19b-3p,hsa-miR-185-5p
IL4	hsa-miR-340-5p

In our study, for the first time, hWJMSC-Exos were combined with the ACECM scaffold, with a suitable structure and composition, to repair osteochondral defects; we explained the possible mechanism by which this combination promotes articular cartilage regeneration from the perspective of Exo-mediated regulation of the articular cavity microenvironment.

The overall results show that the reparative effect in the Exo + S group was significantly better than those in the other three groups, close to the level in the sham group (normal cartilage). According to the macroscopic performance and scores, the new cartilage in the Exo + S group was not tightly integrated with the surrounding normal cartilage at 3 months. At 6 months, the new cartilage showed no obvious boundary with the surrounding normal cartilage. This proves that cartilage repair may gradually proceed from the center to the periphery.

It is worth noting that the direction of cellular arrangement in deep cartilage tissue is perpendicular to the subchondral bone [56]. In the Exo + S and PBS + S groups, with the ACECM scaffold, histomorphological staining showed that the deep cells were arranged in a typical vertical band, similar to the cellular arrangement in natural cartilage. This is similar to the previous research results reported by Zheng X [57] and Guo W [58]. The cells in the repaired tissue in the Exo group were arranged in a disorderly manner, which was significantly different from the normal cartilage structure. This may be one of the reasons why the Young's modulus in the Exo group was lower than that in the Exo + S group. At 6 months, the Young's modulus in the Exo + S group was similar to that in the sham group. Young's modulus is one of the main differences between hyaline cartilage and fibrocartilage. At present, the most commonly used clinical cartilage repair techniques can induce the formation of only fibrocartilage, with a low Young's modulus [59], resulting in insufficient cartilage durability. The Exo + S group in this study showed the potential to solve this problem, which is consistent with the results reported by Wong KL et al. [60], who confirmed in the rabbit model that Exos combined with hyaluronic acid can improve the structural and mechanical properties of repaired cartilage.

Another significant feature of hyaline cartilage compared to fibrocartilage is the high content of type II collagen [61]. Immunohistochemical staining revealed obvious and uniform coloration in the Exo + S group, demonstrating the high content of type II collagen in the repaired tissue. Although the quantitative results showed that the collagen content in the Exo + S group was still lower than that of normal cartilage, it was significantly higher than that in the PBS, PBS + S and Exo groups.

A large number of studies have used exosomes as stem cell substitutes or bioactive materials to repair articular cartilage defects. Liu X confirmed that the imine cross-linked hydrogel containing MSC-Exos has the ability to promote cartilage regeneration [55], but the mechanism and role of MSC-Exos in the process of cartilage regeneration are still unclear. Our study confirms that hWJMSC-Exos can promote the migration and proliferation of BMSCs in vitro and can promote the proliferation of chondrocytes, which is consistent with the results of Hu H's research [62]. Studies by Zhang S [63] and Woo CH [47] confirmed that Exos derived from human embryonic stem cell-derived MSCs and human adipose-derived MSCs have similar biological functions. Based on the above evidence, we conclude that the effect of MSC-Exos in promoting the proliferation and migration of BMSCs and chondrocytes may be universal, regardless of the source of MSCs from which the Exos are derived.

On the basis of in vitro experiments, we applied a rat osteochondral defect model to explore the effect of hWJMSC-Exos on the migration of BMSCs in vivo. Immunofluorescence stainingshowed that the number of MSCs in the defect site in the Exo group was greater than that in the PBS group, but the difference between the two groups was not significant. It is worth noting that there were few MSCs in the center of the cartilage defect in the two groups, and most MSCs were concentrated at the edge of the defect. We may consider the following reasons to explain this phenomenon: (1) The migration and differentiation of MSCs in the body is a dynamic process. The migration of MSCs caused by the injection of Exos on the 7th and 14th days may not have been captured on the 10th and 20th days. It is possible that the migrated MSCs had already differentiated by these time points. (2) Mild subchondral bone injury may limit the migration of BMSCs to the defect site. The osteochondral defect did not completely penetrate the subchondral bone, and no microfracture procedure was performed, so the migration of BMSCs to the defect location was not unobstructed. The edge of the trephine we used for modeling caused deeper defects, so the stem cells that migrated were almost all concentrated at the edge of the defect.

Inflammation has an important impact on the process of tissue repair and regeneration, and synovial inflammation is closely related to the occurrence and development of OA [64]. M2-type macrophages regulate the tissue inflammatory microenvironment by secreting IL-10 and other anti-inflammatory cytokines [65], which are conducive to tissue regeneration and repair. Researchers have long discovered that MSCs can regulate the immune response and inhibit inflammation [66]. Immunofluorescence staining confirmed that the injection of MSC-Exos into the articular cavity can significantly promote the polarization of macrophages toward the M2 phenotype, leading to increased IL-10 secretion and thereby inhibiting inflammation. This may be one of the mechanisms by which MSC-Exos mediate articular cartilage regeneration.

miRNAs are small noncoding RNAs that regulate gene expression by recognizing homologous sequences and interfering with transcription, translation, or epigenetic processes [67]. miRNA sequencing and analysis revealed miRNAs in hWJMSC-Exos that can promote cartilage matrix synthesis and cartilage regeneration. In addition, through target gene prediction, we identified 20 miRNAs that have a beneficial effect on regulating the microenvironment of the joint cavity. Functional enrichment analysis of the top 50 high-abundance miRNAs according to the total read count identified the most significant biological signaling pathways. This narrows the scope for further determining the molecular mechanism of hWJMSC-Exos in the cartilage repair process and provides a reference for determining new cartilage regeneration regulation targets.

Interestingly, although the PBS + S group was better than the Exo group in terms of the ICRS score, WORMS, BVF, histomorphology score, Young's modulus, and collagen content, the Exo group was only better than the PBS + S group in terms of the Tb.Th; however, the above-mentioned differences between the two groups were not significant. We believe the reasons for these findings are as follows: Both the ACECM scaffold and Exos can promote osteochondral regeneration. ② Although ACECM may have a stronger effect in terms of promoting osteochondral regeneration, its effect is not significantly different from that of Exos. The ACECM scaffold can promote cell adhesion, proliferation and differentiation into chondrocytes, and it has been proven to be an effective bioactive material scaffold [68]. Exos mainly play a beneficial role in regulating the microenvironment of the joint cavity. From the overall results, the Exo + S group showed the best regenerative effect, better than that in the PBS + S and Exo groups, which proves that the ACECM scaffold and Exos play a synergistic role in the process of osteochondral regeneration.

The micro-CT results showed that the subchondral bone in the Exo + S group was well repaired. The essence of subchondral bone is bone tissue. A large number of studies have proven that miRNAs play an important role in the regeneration of bone tissue [69]. We found that miR26a and miR199a are highly expressed in hWJMSC-Exos, ranking in the top 20 of all miRNAs in terms of abundance. miRNA26a is a very important regulatory RNA for bone regeneration. A study by Li Y [70] has confirmed that it promotes bone regeneration through angiogenesis-osteogenesis coupling. Zhang X [71] delivered miRNA26a through acellular scaffolds to achieve critical-size bone defect repair. miR199a has been proven to improve the osteogenic differentiation of MSCs through the HIF-1α pathway [72]. Finally, it cannot be ignored that our defect model did not completely penetrate the subchondral bone, and the subchondral bone itself has a blood supply; as such, we believe that subchondral bone has its own self-repair mechanism. In summary, the subchondral bone repair may be the result of the combined effects of Exos and self-repair.

Our study confirms that hWJMSC-Exos can enhance the reparative effect of the ACECM scaffold in a rabbit osteochondral defect model. This effect may be attributed to the promotion of endogenous MSC and chondrocyte proliferation, the inhibition of inflammation in the joint cavity, and the promotion of cartilage ECM synthesis by Exos and exosomal miRNAs (Fig. 13). The "cell-free" tissue engineering strategy based on MSC-Exos and the ACECM scaffold is an effective method with which to achieve osteochondral regeneration. In view of the fact that the ACECM scaffold derived from human cartilage matrix has been successfully used in clinical practice, this new type of "cell-free" tissue-engineered cartilage has broad prospects for clinical translation.

Our research also has some limitations. Is the increase in the number of M2-type macrophages caused by Exos only manifested as a decrease in inflammation? Do M2-type macrophages also affect the biological functions of endogenous stem cells or chondrocytes through Exos? These questions may be answered by cocultivating M2-type macrophages with stem cells or chondrocytes in vitro. In addition, we found miRNAs that may play a role in promoting osteochondral regeneration, but it is not clear which miRNA plays a central role. At the same time, we also need to finally determine the signaling pathway and identify a definite molecular target for the clinical realization of osteochondral regeneration. Finally, the exact metabolic process of Exos in the articular cavity is still unclear; thus, there is no uniform standard for the number or interval of Exo administration. This problem requires new experiments to establish an optimal dosing regimen. The above questions are worthy of in-depth

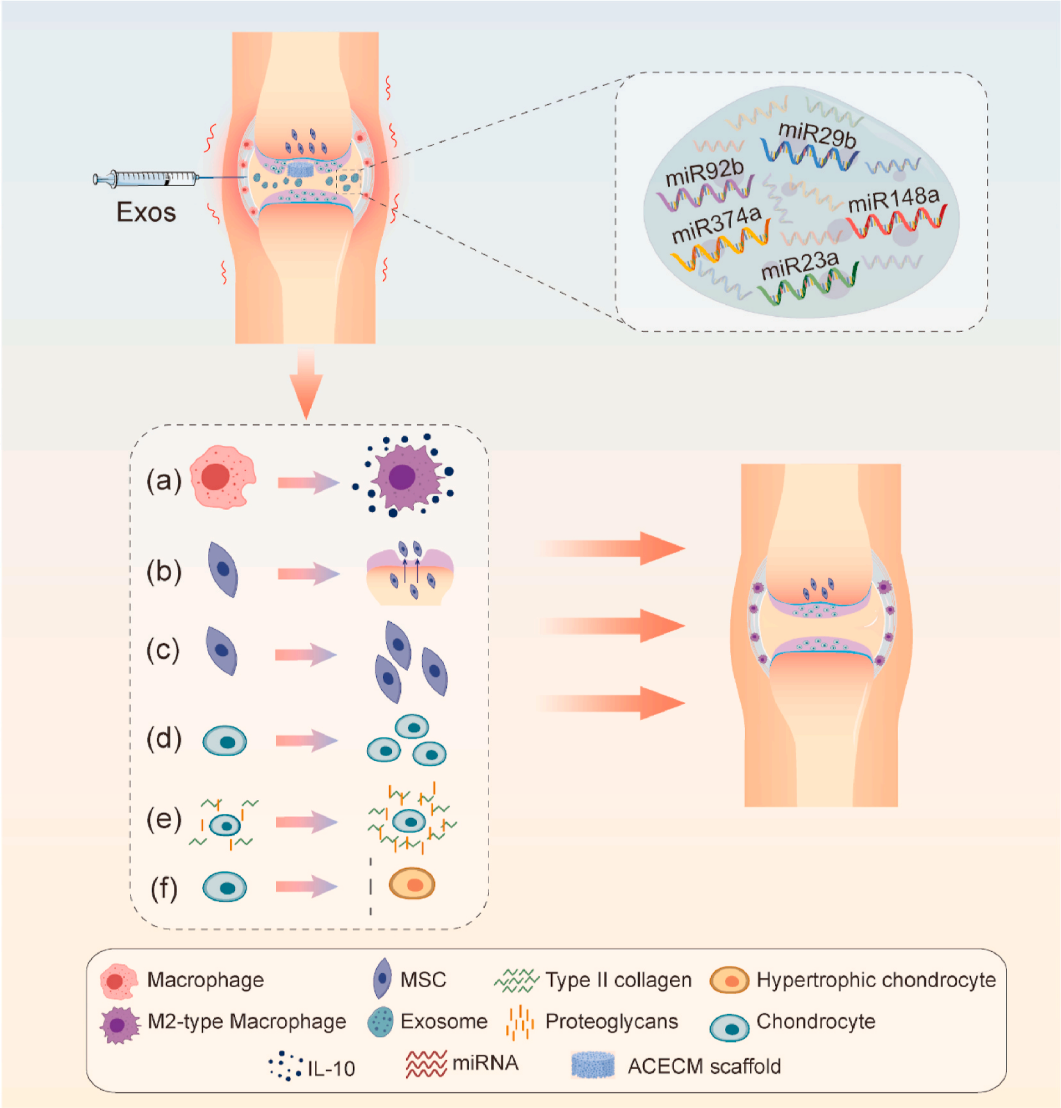

Fig. 13. The possible mechanism of MSC-Exos promoting osteochondral regeneration. (a) Promoting macrophage polarization toward the M2 phenotype. (b) Promoting MSC migration. (c) Promoting MSC proliferation. (d) Promoting chondrocyte proliferation. (e) Promoting the secretion of cartilage matrix. (f) inhibiting chondrocyte hypertrophy.

discussion in a new study.

5. Conclusion

hWJMSC-Exos can promote osteochondral regeneration. This effect may be attributed to the inhibition of joint cavity inflammation by Exos and the promotion of cartilage ECM synthesis by exosomal miRNAs. The "cell-free" tissue engineering strategy based on MSC-Exos and the ACECM scaffold is an effective method with which to achieve osteochondral regeneration. This study provides an important theoretical basis for the development of "cell-free" tissue-engineered cartilage.

CRediT authorship contribution statement

Shuangpeng Jiang: Writing - original draft, Investigation, Data curation, Formal analysis, Visualization. **Guangzhao Tian:** Investigation, Data curation. **Zhen Yang:** Investigation, Formal analysis. **Xiang Gao:** Data curation, Formal analysis. **Fuxin Wang:** Data curation. **Juntan Li:** Formal analysis. **Zhuang Tian:** Methodology. **Bo Huang:** Software. **Fu Wei:** Investigation. **Xinyu Sang:** Methodology. **Liuqi Shao:** Investigation. **Jian Zhou:** Investigation, Methodology. **Zhenyong Wang:** Investigation, Methodology. **Shuyun Liu:** Methodology, Project administration. **Xiang Sui:** Resources. **Quanyi Guo:** Supervision. **Weimin Guo:** Supervision. **Xu Li:** Conceptualization, Supervision.

Declaration of competing interest

The authors declare that there are no conflicts of interest.

Acknowledgments

This work was supported by the National Key R&D Program of China (2019 YFA 0110600), the National Natural Science Foundation of China (81772319), the Scientific Research Funding Project of Education Department of Liaoning Province (JC2019001) and the China Postdoctoral Science Foundation (2020M681010).

Appendix A. Supplementary data

Supplementary data related to this article can be found at https://doi.org/10.1016/j.bioactmat.2021.01.031.

References

[1] G. Musumeci, M.L. Carnazza, C. Loreto, R. Leonardi, C. Loreto, β-Defensin-4 (HBD-4) is expressed in chondrocytes derived from normal and osteoarthritic cartilage encapsulated in PEGDA scaffold, Acta Histochem. 114 (2012) 805–812, https://doi.org/10.1016/j.acthis.2012.02.001.

[2] M. Brittberg, A.H. Gomoll, J.A. Canseco, J. Far, M. Lind, J. Hui, Cartilage repair in the degenerative ageing knee, Acta Orthop. 87 (2016) 26–38, https://doi.org/10.1080/17453674.2016.1265877.

[3] D.J. Hunter, S. Bierma-Zeinstra, Osteoarthritis, Lancet 393 (2019) 1745–1759, https://doi.org/10.1016/S0140-6736(19)30417-9.

[4] S.A. Muhammad, N. Nordin, M.Z. Mehat, S. Fakurazi, Comparative efficacy of stem cells and secretome in articular cartilage regeneration: a systematic review and meta-analysis, Cell Tissue Res. 375 (2019) 329–344, https://doi.org/10.1007/s00441-018-2884-0.

[5] C.R. Harrell, B.S. Markovic, C. Fellabaum, A. Arsenijevic, V. Volarevic, Mesenchymal stem cell-based therapy of osteoarthritis: current knowledge and future perspectives, Biomed. Pharmacother. 109 (2019) 2318–2326, https://doi.org/10.1016/j.biopha.2018.11.099.

[6] L. Reppel, J. Schiavi, N. Charif, et al., Chondrogenic induction of mesenchymal stromal/stem cells from Wharton's jelly embedded in alginate hydrogel and without added growth factor: an alternative stem cell source for cartilage tissue engineering, Stem Cell Res. Ther. 6 (2015) 260, https://doi.org/10.1186/s13287-015-0263-2.

[7] A. Lindenmair, T. Hatlapatka, G. Kollwig, et al., Mesenchymal stem or stromal cells from amnion and umbilical cord tissue and their potential for clinical applications, Cells 1 (2012) 1061–1088, https://doi.org/10.3390/cells1041061.

[8] T. Li, M. Xia, Y. Gao, Y. Chen, Y. Xu, Human umbilical cord mesenchymal stem cells: an overview of their potential in cell-based therapy, Expet Opin. Biol. Ther. 15 (2015) 1293–1306, https://doi.org/10.1517/14712598.2015.1051528.

[9] Ž. Večerić-Haler, A. Cerar, M. Perše, (Mesenchymal) stem cell-based therapy in cisplatin-induced acute kidney injury animal model: risk of immunogenicity and tumorigenicity, Stem Cell. Int. 2017 (2017) 7304643, https://doi.org/10.1155/2017/7304643.

[10] L. Barkholt, E. Flory, V. Jekerle, et al., Risk of tumorigenicity in mesenchymal stromal cell-based therapies–bridging scientific observations and regulatory viewpoints, Cytotherapy 15 (2013) 753–759, https://doi.org/10.1016/j.jcyt.2013.03.005.

[11] P. Neviani, P.M. Wise, M. Murtadha, et al., Natural killer-derived exosomal miR-186 inhibits neuroblastoma growth and immune escape mechanisms, Canc. Res. 79 (2019) 1151–1164, https://doi.org/10.1158/0008-5472.CAN-18-0779.

[12] W. Li, L.Y. Jin, Y.B. Cui, N. Xie, Human umbilical cord mesenchymal stem cells-derived exosomal microRNA-17-3p ameliorates inflammatory reaction and antioxidant injury of mice with diabetic retinopathy via targeting STAT1, Int. Immunopharm. 90 (2020) 107010, https://doi.org/10.1016/j.intimp.2020.107010.

[13] C. Zhang, Z. Zhu, J. Gao, et al., Plasma exosomal miR-375-3p regulates mitochondria-dependent keratinocyte apoptosis by targeting XIAP in severe drug-induced skin reactions, Sci. Transl. Med. 12 (2020), https://doi.org/10.1126/scitranslmed.aaw6142.

[14] Y. Zhang, J. Zhao, M. Ding, et al., Loss of exosomal miR-146a-5p from cancer-associated fibroblasts after androgen deprivation therapy contributes to prostate cancer metastasis, J. Exp. Clin. Canc. Res. 39 (2020) 282, https://doi.org/10.1186/s13046-020-01761-1.

[15] S. Keshtkar, N. Azarpira, M.H. Ghahremani, Mesenchymal stem cell-derived extracellular vesicles: novel frontiers in regenerative medicine, Stem Cell Res. Ther. 9 (2018) 63, https://doi.org/10.1186/s13287-018-0791-7.

[16] S. Cosenza, M. Ruiz, K. Toupet, C. Jorgensen, D. Noël, Mesenchymal stem cells derived exosomes and microparticles protect cartilage and bone from degradation in osteoarthritis, Sci. Rep. 7 (2017) 16214, https://doi.org/10.1038/s41598-017-15376-8.

[17] D.G. Phinney, M.F. Pittenger, Concise review: MSC-derived exosomes for cell-free therapy, Stem Cell. 35 (2017) 851–858, https://doi.org/10.1002/stem.2575.

[18] D. Burger, J.L. Viñas, S. Akbari, et al., Human endothelial colony-forming cells protect against acute kidney injury: role of exosomes, Am. J. Pathol. 185 (2015) 2309–2323, https://doi.org/10.1016/j.ajpath.2015.04.010.

[19] H. Xin, Y. Li, M. Chopp, Exosomes/miRNAs as mediating cell-based therapy of stroke, Front. Cell. Neurosci. 8 (2014) 377, https://doi.org/10.3389/fncel.2014.00377.

[20] S. Zhang, W.C. Chu, R.C. Lai, S.K. Lim, J.H. Hui, W.S. Toh, Exosomes derived from human embryonic mesenchymal stem cells promote osteochondral regeneration, Osteoarthr, Cartil 24 (2016) 2135–2140, https://doi.org/10.1016/j.joca.2016.06.022.

[21] S.C. Tao, T. Yuan, Y.L. Zhang, W.J. Yin, S.C. Guo, C.Q. Zhang, Exosomes derived from miR-140-5p-overexpressing human synovial mesenchymal stem cells enhance cartilage tissue regeneration and prevent osteoarthritis of the knee in a rat model, Theranostics 7 (2017) 180–195, https://doi.org/10.7150/thno.17133.

[22] X. Wu, Y. Wang, Y. Xiao, R. Crawford, X. Mao, I. Prasadam, Extracellular vesicles: potential role in osteoarthritis regenerative medicine, J. Orthop. Translat. 21 (2020) 73–80, https://doi.org/10.1016/j.jot.2019.10.012.

[23] Q. Yang, J. Peng, Q. Guo, et al., A cartilage ECM-derived 3-D porous acellular matrix scaffold for in vivo cartilage tissue engineering with PKH26-labeled chondrogenic bone marrow-derived mesenchymal stem cells, Biomaterials 29 (2008) 2378–2387, https://doi.org/10.1016/j.biomaterials.2008.01.037.

[24] H. Kang, J. Peng, S. Lu, et al., In vivo cartilage repair using adipose-derived stem cell-loaded decellularized cartilage ECM scaffolds, J. Tissue Eng. Regen. Med. 8 (2014) 442–453, https://doi.org/10.1002/term.1538.

[25] N. Ma, H. Wang, X. Xu, et al., Autologous-cell-derived, tissue-engineered cartilage for repairing articular cartilage lesions in the knee: study protocol for a randomized controlled trial, Trials 18 (2017) 519, https://doi.org/10.1186/s13063-017-2251-6.

[26] Y. Zhang, S. Liu, W. Guo, et al., Coculture of hWJMSCs and pACs in oriented scaffold enhances hyaline cartilage regeneration in vitro, Stem Cell. Int. 2019 (2019) 5130152, https://doi.org/10.1155/2019/5130152.

[27] Z. Yuan, S. Liu, C. Hao, et al., AMECM/DCB scaffold prompts successful total meniscus reconstruction in a rabbit total meniscectomy model, Biomaterials 111 (2016) 13–26, https://doi.org/10.1016/j.biomaterials.2016.09.017.

[28] M.P. van den Borne, N.J. Raijmakers, J. Vanlauwe, et al., International cartilage repair society (ICRS) and oswestry macroscopic cartilage evaluation scores validated for use in autologous chondrocyte implantation (ACI) and microfracture, Osteoarthritis Cartilage 15 (2007) 1397–1402, https://doi.org/10.1016/j.joca.2007.05.005.

[29] C.G. Peterfy, A. Guermazi, S. Zaim, et al., Whole-organ magnetic resonance imaging score (WORMS) of the knee in osteoarthritis, Osteoarthritis Cartilage 12 (2004) 177–190, https://doi.org/10.1016/j.joca.2003.11.003.

[30] R. Leonardi, C. Loreto, E. Barbato, et al., MMP-13 (collagenase 3) localization in human temporomandibular joint discs with internal derangement, Acta Histochem. 110 (2008) 314–318, https://doi.org/10.1016/j.acthis.2007.11.010.

[31] R. Leonardi, M.C. Rusu, F. Loreto, C. Loreto, G. Musumeci, Immunolocalization and expression of lubricin in the bilaminar zone of the human temporomandibular joint disc, Acta Histochem. 114 (2012) 1–5, https://doi.org/10.1016/j.acthis.2010.11.011.

[32] X. Guo, H. Park, S. Young, et al., Repair of osteochondral defects with biodegradable hydrogel composites encapsulating marrow mesenchymal stem cells in a rabbit model, Acta Biomater. 6 (2010) 39–47, https://doi.org/10.1016/j.actbio.2009.07.041.

[33] J.I. Wolfstadt, B.J. Cole, D.J. Ogilvie-Harris, S. Viswanathan, J. Chahal, Current concepts: the role of mesenchymal stem cells in the management of knee osteoarthritis, Sport Health 7 (2015) 38–44, https://doi.org/10.1177/1941738114529727.
[34] L.A. Vonk, A.H. Kragten, W.J. Dhert, D.B. Saris, L.B. Creemers, Overexpression of hsa-miR-148a promotes cartilage production and inhibits cartilage degradation by osteoarthritic chondrocytes, Osteoarthritis Cartilage 22 (2014) 145–153, https://doi.org/10.1016/j.joca.2013.11.006.
[35] U. Mayer, A. Benditz, S. Grässel, miR-29b regulates expression of collagens I and III in chondrogenically differentiating BMSC in an osteoarthritic environment, Sci. Rep. 7 (2017) 13297, https://doi.org/10.1038/s41598-017-13567-x.
[36] N. Akhtar, T.M. Haqqi, MicroRNA-199a* regulates the expression of cyclooxygenase-2 in human chondrocytes, Ann. Rheum. Dis. 71 (2012) 1073–1080, https://doi.org/10.1136/annrheumdis-2011-200519.
[37] T. Matsukawa, T. Sakai, T. Yonezawa, et al., MicroRNA-125b regulates the expression of aggrecanase-1 (ADAMTS-4) in human osteoarthritic chondrocytes, Arthritis Res. Ther. 15 (2013) R28, https://doi.org/10.1186/ar4164.
[38] J. Xu, Y. Liu, M. Deng, et al., MicroRNA221-3p modulates Ets-1 expression in synovial fibroblasts from patients with osteoarthritis of temporomandibular joint, Osteoarthritis Cartilage 24 (2016) 2003–2011, https://doi.org/10.1016/j.joca.2016.06.011.
[39] G. Mao, Z. Zhang, Z. Huang, et al., MicroRNA-92a-3p regulates the expression of cartilage-specific genes by directly targeting histone deacetylase 2 in chondrogenesis and degradation, Osteoarthritis Cartilage 25 (2017) 521–532, https://doi.org/10.1016/j.joca.2016.11.006.
[40] X. Lin, L. Chen, H. Li, et al., miR-155 accelerates proliferation of mouse hepatocytes during liver regeneration by directly targeting SOCS1, Am. J. Physiol. Gastrointest. Liver Physiol. 315 (2018) G443–443G453, https://doi.org/10.1152/ajpgi.00072.2018.
[41] Y. Bei, Y. Song, F. Wang, et al., miR-382 targeting PTEN-Akt axis promotes liver regeneration, Oncotarget 7 (2016) 1584–1597, https://doi.org/10.18632/oncotarget.6444.
[42] R.R. Chivukula, G. Shi, A. Acharya, et al., An essential mesenchymal function for miR-143/145 in intestinal epithelial regeneration, Cell 157 (2014) 1104–1116, https://doi.org/10.1016/j.cell.2014.03.055.
[43] A. Eulalio, M. Mano, M. Dal Ferro, et al., Functional screening identifies miRNAs inducing cardiac regeneration, Nature 492 (2012) 376–381, https://doi.org/10.1038/nature11739.
[44] K.H. Lu, A. Tounsi, N. Shridhar, et al., Dickkopf-3 contributes to the regulation of anti-tumor immune responses by mesenchymal stem cells, Front. Immunol. 6 (2015) 645, https://doi.org/10.3389/fimmu.2015.00645.
[45] X.T. He, X. Li, Y. Xia, et al., Building capacity for macrophage modulation and stem cell recruitment in high-stiffness hydrogels for complex periodontal regeneration: experimental studies in vitro and in rats, Acta Biomater. 88 (2019) 162–180, https://doi.org/10.1016/j.actbio.2019.02.004.
[46] W. Zhou, S.Q. Ke, Z. Huang, et al., Periostin secreted by glioblastoma stem cells recruits M2 tumour-associated macrophages and promotes malignant growth, Nat. Cell Biol. 17 (2015) 170–182, https://doi.org/10.1038/ncb3090.
[47] C.H. Woo, H.K. Kim, G.Y. Jung, et al., Small extracellular vesicles from human adipose-derived stem cells attenuate cartilage degeneration, J. Extracell. Vesicles 9 (2020) 1735249, https://doi.org/10.1080/20013078.2020.1735249.
[48] L. Li, X. Duan, Z. Fan, et al., Mesenchymal stem cells in combination with hyaluronic acid for articular cartilage defects, Sci. Rep. 8 (2018) 9900, https://doi.org/10.1038/s41598-018-27737-y.
[49] D. Zhao, T. Zhu, J. Li, et al., Poly(lactic-co-glycolic acid)-based composite bone-substitute materials, Bioact. Mater. 6 (2021) 346–360, https://doi.org/10.1016/j.bioactmat.2020.08.016.
[50] T. Zhu, Y. Cui, M. Zhang, D. Zhao, G. Liu, J. Ding, Engineered three-dimensional scaffolds for enhanced bone regeneration in osteonecrosis, Bioact. Mater. 5 (2020) 584–601, https://doi.org/10.1016/j.bioactmat.2020.04.008.
[51] Y. Zhang, J. Yu, K. Ren, J. Zuo, J. Ding, X. Chen, Thermosensitive hydrogels as scaffolds for cartilage tissue engineering, Biomacromolecules 20 (2019) 1478–1492, https://doi.org/10.1021/acs.biomac.9b00043.
[52] Y. Zhang, X. Liu, L. Zeng, et al., Polymer fiber scaffolds for bone and cartilage tissue engineering, Adv. Funct. Mater. 29 (2019) 1903279.1–1903279.20.
[53] Chenyu, Wang, Naibo, et al., Cartilage repair: injectable cholesterol-enhanced stereocomplex polylactide thermogel loading chondrocytes for optimized cartilage regeneration (adv. Healthcare mater. 14/2019), Adv. Healthc. Mater. 8 (2019), 1970056-1970056.
[54] Q. Meng, X. Hu, H. Huang, et al., Microfracture combined with functional pig peritoneum-derived acellular matrix for cartilage repair in rabbit models, Acta Biomater. 53 (2017) 279–292, https://doi.org/10.1016/j.actbio.2017.01.055.
[55] L. Xiaolin, Y. Yunlong, L. Yan, et al., Integration of stem cell-derived exosomes with in situ hydrogel glue as a promising tissue patch for articular cartilage regeneration, Nanoscale 9 (2017).
[56] S. Camarero-Espinosa, B. Rothen-Rutishauser, E.J. Foster, C. Weder, Articular cartilage: from formation to tissue engineering, Biomater. Sci. 4 (2016) 734–767, https://doi.org/10.1039/c6bm00068a.
[57] X. Zheng, F. Yang, S. Wang, et al., Fabrication and cell affinity of biomimetic structured PLGA/articular cartilage ECM composite scaffold, J. Mater. Sci. Mater. Med. 22 (2011) 693–704, https://doi.org/10.1007/s10856-011-4248-0.
[58] W. Guo, X. Zheng, W. Zhang, et al., Mesenchymal stem cells in oriented PLGA/ACECM composite scaffolds enhance structure-specific regeneration of hyaline cartilage in a rabbit model, Stem Cell. Int. 2018 (2018) 6542198, https://doi.org/10.1155/2018/6542198.
[59] S. Jiang, W. Guo, G. Tian, et al., Clinical application status of articular cartilage regeneration techniques: tissue-engineered cartilage brings new hope, Stem Cell. Int. 2020 (2020) 5690252, https://doi.org/10.1155/2020/5690252.
[60] K.L. Wong, S. Zhang, M. Wang, et al., Intra-articular injections of mesenchymal stem cell exosomes and hyaluronic acid improve structural and mechanical properties of repaired cartilage in a rabbit model, Arthroscopy 36 (2020) 2215–2228, https://doi.org/10.1016/j.arthro.2020.03.031, e2.
[61] Y. Shi, X. Hu, J. Cheng, et al., A small molecule promotes cartilage extracellular matrix generation and inhibits osteoarthritis development, Nat. Commun. 10 (2019) 1914, https://doi.org/10.1038/s41467-019-09839-x.
[62] H. Hu, L. Dong, Z. Bu, et al., miR-23a-3p-abundant small extracellular vesicles released from Gelma/nanoclay hydrogel for cartilage regeneration, J. Extracell. Vesicles 9 (2020) 1778883, https://doi.org/10.1080/20013078.2020.1778883.
[63] S. Zhang, S.J. Chuah, R.C. Lai, J. Hui, S.K. Lim, W.S. Toh, MSC exosomes mediate cartilage repair by enhancing proliferation, attenuating apoptosis and modulating immune reactivity, Biomaterials 156 (2018) 16–27, https://doi.org/10.1016/j.biomaterials.2017.11.028.
[64] J. Sellam, F. Berenbaum, The role of synovitis in pathophysiology and clinical symptoms of osteoarthritis, Nat. Rev. Rheumatol. 6 (2010) 625–635, https://doi.org/10.1038/nrrheum.2010.159.
[65] A. Shapouri-Moghaddam, S. Mohammadian, H. Vazini, et al., Macrophage plasticity, polarization, and function in health and disease, J. Cell. Physiol. 233 (2018) 6425–6440, https://doi.org/10.1002/jcp.26429.
[66] S. Aggarwal, M.F. Pittenger, Human mesenchymal stem cells modulate allogeneic immune cell responses, Blood 105 (2005) 1815–1822, https://doi.org/10.1182/blood-2004-04-1559.
[67] L. Chen, L. Heikkinen, C. Wang, Y. Yang, H. Sun, G. Wong, Trends in the development of miRNA bioinformatics tools, Briefings Bioinf. 20 (2019) 1836–1852, https://doi.org/10.1093/bib/bby054.
[68] X. Sun, H. Yin, Y. Wang, et al., In situ articular cartilage regeneration through endogenous reparative cell homing using a functional bone marrow-specific scaffolding system, ACS Appl. Mater. Interfaces 10 (2018) 38715–38728, https://doi.org/10.1021/acsami.8b11687.
[69] L. Hong, H. Sun, B.A. Amendt, MicroRNA function in craniofacial bone formation, regeneration and repair, Bone 144 (2020) 115789, https://doi.org/10.1016/j.bone.2020.115789.
[70] Y. Li, L. Fan, S. Liu, et al., The promotion of bone regeneration through positive regulation of angiogenic-osteogenic coupling using microRNA-26a, Biomaterials 34 (2013) 5048–5058, https://doi.org/10.1016/j.biomaterials.2013.03.052.
[71] X. Zhang, Y. Li, Y.E. Chen, J. Chen, P.X. Ma, Cell-free 3D scaffold with two-stage delivery of miRNA-26a to regenerate critical-sized bone defects, Nat. Commun. 7 (2016) 10376, https://doi.org/10.1038/ncomms10376.
[72] X. Chen, S. Gu, B.F. Chen, et al., Nanoparticle delivery of stable miR-199a-5p agomir improves the osteogenesis of human mesenchymal stem cells via the HIF1a pathway, Biomaterials 53 (2015) 239–250, https://doi.org/10.1016/j.biomaterials.2015.02.071.